DOI: 10.1002/ejic.200700070

Synthetic, X-ray Diffraction, Electrochemical, and Density Functional Theoretical Studies of (Indenyl)ruthenium Complexes Containing Dithiolate Ligands

Sin Yee Ng,[a] Jialin Tan,[a] Wai Yip Fan,[a] Weng Kee Leong,[a] Lai Yoong Goh,*[a] and Richard D. Webster[b]

Keywords: Ruthenium complexes / Dithiolates / Cyclic voltammetry / Density functional calculations

Halide substitution of the complexes [(Ind)Ru(L_2)X] {Ind = η^5-C_9H_7. **1**: (L_2) = dppf [1,1′-bis(diphenylphosphanyl)ferrocene], X = Cl; **2**: (L_2) = dppm [1,1′-bis(diphenylphosphanyl)methane], X = Cl; and **18**: (L_2) = $(CO)_2$, X = I} with the 1,1-dithiolates $^-S_2CNR_2$ (dialkyl dithiocarbamates for R = Me, Et, and C_5H_{10}), ^-S_2COR (alkyl xanthates for R = Et and *i*Pr), and $^-S_2PR_2$ (dithiophosphinates for R = Et and Ph) showed that the lability of the indenyl ligand is influenced by the nature of both the coligand and the incoming dithiolate, as well as the solvent. In addition to dithiolate derivatives, the reactions also produced the hydride species [(Ind)Ru(diphos)H] in solvent- and stoichiometry-dependent yields. The observed dependence of lability of Ind on (L_2) follows the order, dppf < dppm ≈ $(CO)_2$, in agreement with the electron-donor capability of L_2, as well as the estimation of lowest activation energy for the $\eta^5 \rightarrow \eta^3$ ring slippage process in the series of complexes [(Ind)Ru$(L)_2(S_2COMe)$] (L = $PMeH_2$, PH_3, CO) for L = CO. The computational study also indicated an indenyl lability order for dithiolate substitution (dithiocarbamate > xanthate), in agreement with experimental findings. The dissociation of the indenyl ligand in chloro substitution of **1** by $^-S_2CNEt_2$ was found to be exhaustive in a polar solvent like MeOH, but only partial in CH_2Cl_2. Cyclic voltammetry experiments indicated that [(Ind)Ru(dppf)(η^1-S_2COiPr)] (**10**) and [(Ind)Ru(dppf)(η^1-S_2PPh_2)] (**13**) can be oxidized in one-electron chemical irreversible or chemical reversible processes, respectively (at a scan rate of 100 mV/s), at about 0 V versus Fc/Fc^+. Complex **13** underwent additional one-electron oxidation processes at +0.5 and +0.8 V versus Fc/Fc^+. The new complexes have all been characterized spectroscopically, and some (four containing the indenyl ligand and three of the non-indenyl type) by X-ray diffraction as well.

Introduction

1,1-Dithiolate compounds represent a class of versatile ligands, owing to the occurrence of resonance phenomena, which result in electron delocalization, as depicted in Scheme 1. Their coordination chemistry with the transition metals commands much interest, on account of the rich diversity of the complexes and their numerous and potential applications in industry and agriculture.[1]

Our work on some of these ligands was directed at their reactivity in the coordination environment of $CpCr(CO)_n$ (n = 2 or 3),[2] (HMB)Ru(dppf), and CpRu(dppf) (Cp = η^5-C_5H_5 and HMB = η^6-C_6Me_6).[3] A logical and interesting follow-up of these studies on Ru would be a corresponding reactivity study of the indenyl (Ind) analogue, as Ind can potentially assume bonding modes involving η^5-Cp or by

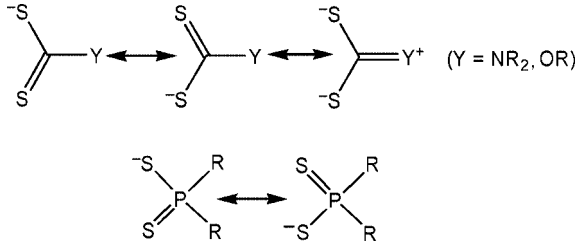

Scheme 1.

ring slippage to η^3 or η^6-C_9H_7.[4] Such an investigation is also timely, as there is intense interest in reactivity aspects of (Ind)Ru complexes, especially from catalytic perspectives;[5] and the bulk of the literature on (Ind)Ru complexes deals with examples containing phosphanes as coligands, with only two such complexes carrying S-donor ligands, viz. SEt and SEtMe.[6] Moreover, the outcome of the study will provide a useful comparison to our completed study of (Ind)Ru(dppf)Cl (**1**) with simple alkyl/aryl monothiolates, SR^- (R = Me, Et, and Ph).[7] This paper will describe the results of reactions of **1**, its dppm analogue **2**, and (Ind)-$Ru(CO)_2I$ **18** with dialkyl dithiocarbamate, alkyl xanthate, and bis(alkyl/aryl)dithiophosphinate, together with X-ray

[a] Department of Chemistry, National University of Singapore, Kent Ridge, Singapore 117543, Singapore
Fax: +65-6779-1691
E-mail: chmgohly@nus.edu.sg
[b] Division of Chemistry and Biological Chemistry, Nanyang Technological University, Singapore 637616, Singapore
Supporting information for this article is available on the WWW under http://www.eurjic.org or from the author.

structural and electrochemical data of some of the new complexes, and a computational estimation of the energies involved in $\eta^5 \rightarrow \eta^3$ ring slippage of the indenyl ligand in selected molecules.

Results and Discussion

Reactions of [(Ind)Ru(L_2)Cl] (L_2 = dppf, dppm)

Reaction with Dialkyl Dithiocarbamates

Complex [(Ind)Ru(dppf)Cl] (**1**) and its dppm analogue [(Ind)Ru(dppm)Cl] (**2**) were reacted with NaS_2CNR_2. The product mixture from the reaction of **1** in MeOH is both stoichiometry- and time-dependent. Thus the addition of 1 mol-equiv. of $^-S_2CNR_2$ to **1** gives complexes [Ru(η^2-dppf)(η^2-S_2CNR_2)$_2$] [R = Me (**3**), Et (**4**), C_5H_{10} (**5**)], together with the hydride, [(Ind)Ru(dppf)H] **6**, which was not observed with the use of excess $^-S_2CNR_2$ (Scheme 2). The release of indene in all cases is consistent with the formation of the non-indenyl complexes **3**–**5**. In the reaction of **1** with 1 mol-equiv. of $^-S_2CNEt_2$, ^{31}P NMR spectroscopy showed that the reaction mixture contained species **1** (δ = 51.7 ppm), **6** (δ = 62.8 ppm), **4** (δ = 47.1 ppm), and [(Ind)-Ru(η^1-dppf)(η^2-S_2CNEt_2)] **4a** (δ = –17.7 and 57.3), in an approximate 2:3:7:1 molar proportion after 4 h at room temperature, but finally only complexes **4** and **6** in 3:2 molar ratio after 16 h. A repeat of the reaction in CH_2Cl_2 using **1** and NaS_2CNEt_2 in 1:4 molar proportion yielded a final 1:1 molar mixture of **4** and **4a**, which was isolated in 35% yield. It was further demonstrated that the reaction of **4a** with NaS_2CNEt_2 in MeOH yielded **4** (Scheme 3).

The structure of **4a** was determined by X-ray diffraction analysis. This is consistent with its NMR spectroscopic data, which indicated the presence of η^5-Ind and η^2-S_2CNEt_2 ligands in the proton spectrum, and η^1-dppf in the ^{31}P spectrum (δ = –17.7 and 57.3, with the upfield signal associated with the uncoordinated phosphorus atom).

The progression of **1** to **4** via **4a** indicates the weaker thermodynamic stability of bidentate dppf versus $^-S_2CNEt_2$, which in excess will also displace the indenyl ligand, accompanied by rechelation of the monodentate dppf ligand in **4a** to achieve the favored hexacoordination at

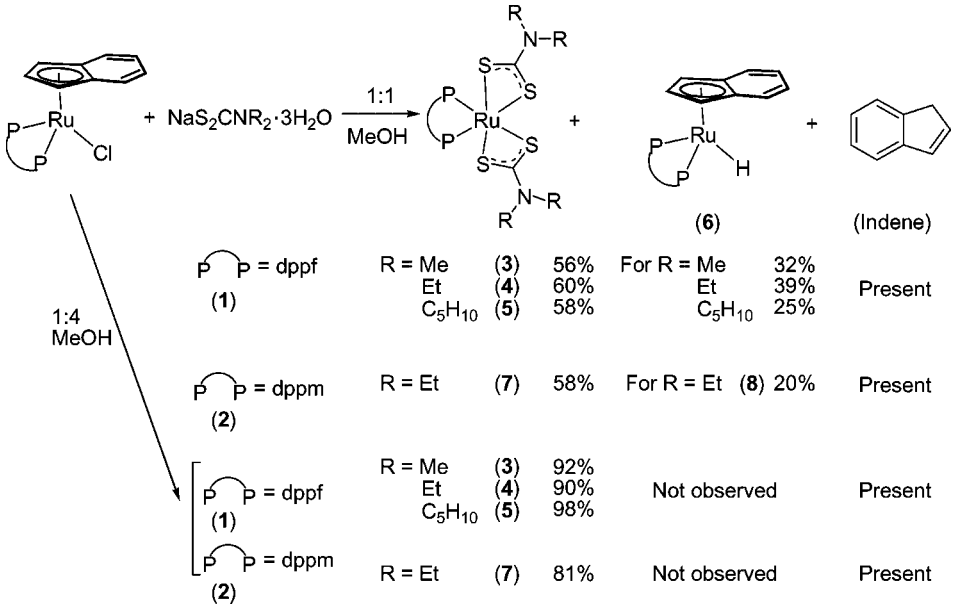

Scheme 2.

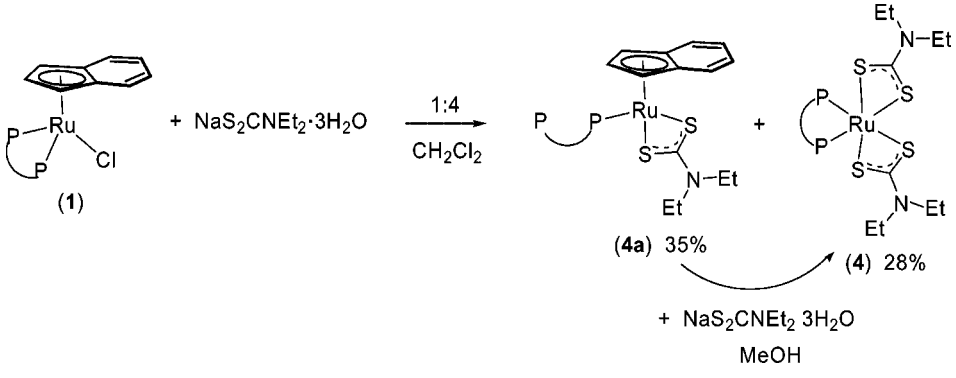

Scheme 3.

Ru^{II}. We had previously isolated complex **4** in 80% yield by displacement of triphenylphosphane in $Ru(\eta^2\text{-}S_2CNEt_2)_2(PPh_3)_2$ with dppf and have observed mono- and bidentate exchange behavior of the dithiocarbamate ligand in solution.[8]

The formation of **6** points to the role of methoxide arising from an equilibrium, as discussed before for SR^- (R = Me, Et):[7]

$$^-S_2CNR_2 + MeOH \overset{K}{\rightleftharpoons} {}^-OMe + HS_2CNR_2$$

It is significant that **6** was not detected when excess $^-S_2CNR_2$ was used. Although it is probable that it was formed but underwent a facile H^- and $^-S_2CNEt_2$ exchange, as found in the reactions of $CpRu(PPh_3)_2H$ with the halide and SCN anions,[9] this probability was ruled out experimentally in this case, as **6** did not react at all with excess NaS_2CNR_2, indicating that **6** was not the intermediate leading to **4**. As the formation of **4** requires 2 mole equiv. of $^-S_2CNEt_2$ to **1**, such a stoichiometric reaction was carried out in MeOH, in an attempt to further investigate the reaction pathways. A yellow precipitate, identified as **4**, was obtained, while the reaction of the filtrate with a new batch of **1** for 18 h at room temp. generated **6**, indicative of the presence of ^-OMe in the filtrate. This indirectly demonstrated that MeOH was the proton source for the conversion of the indenyl moiety to indene.

A comparative study was carried out on the reactivity of [(Ind)Ru(dppm)Cl] (**2**), the dppm analogue of **1**, towards the nucleophile $^-S_2CNR_2$. As shown in Scheme 2, similar observations were found in MeOH solvent, giving **7** (a compound similar to **4**) and **8** (a hydride similar to **6**);[10] the latter was not formed when the nucleophile was used in excess. However, the dppm equivalent of **4a**, that is, [(Ind)-$Ru(\eta^1\text{-dppm})(\eta^2\text{-}S_2CNEt_2)$], was not observed, probably because of thermodynamic instability, though complexes with monodentate dppm are known.[11]

Our previous studies showed that the outcome of the reactions of LRu(dppf)Cl [L = Cp (**A**), HMB (**B**)] with $^-S_2CNEt_2$ were very different. For L = Cp, a dinuclear complex $[CpRu(S_2CNEt_2)_2]_2(\mu\text{-dppf})$ (**C**) was formed, and for L = arene, $^-S_2CNEt_2$ displaced the arene ligand, as it displaced the indenyl ligand in complex **1**, as discussed above (see Scheme 4, a,b[3a]). In comparison, the analogous reaction of [CpRu(dppe)Cl] (**D**) was reported to give the mononuclear complex $[CpRu(dppe)(\eta^1\text{-}S_2CNEt_2)]$ (**E**) (Scheme 4, c).[12]

Reaction with Alkyl Xanthates

The reaction of **1** with KS_2COR (R = Et, *i*Pr) in MeOH at room temp. or in refluxing CH_2Cl_2 yielded $[(Ind)Ru(\eta^2\text{-dppf})(\eta^1\text{-}S_2COR)]$ in high yield [R = Et (**9**), 78% yield; R = *i*Pr (**10**), 83% yield]. On the other hand, the reaction of **2** with KS_2CO*i*Pr in MeOH gave only a non-indenyl complex $[Ru(\eta^2\text{-dppm})(\eta^2\text{-}S_2CO$*i*$Pr)_2]$ (**11**) (Scheme 5). There was no sign of the formation of any (Ind)Ru complex, neither $[(Ind)Ru(\eta^2\text{-dppm})(\eta^1\text{-}S_2COR)]$ nor $[(Ind)Ru(\eta^1\text{-dppm})(\eta^2\text{-}S_2COR)]$, indicative of thermodynamic instability of such indenyl compounds in MeOH. A change of solvent to CH_2Cl_2 was attempted; however, unlike in the case with $^-S_2CNR_2$, there was no reaction at all, even after prolonged heating.

The ^1H NMR spectra of **9** and **10** showed the presence of η^5-Ind [$\delta(H^2)$ 5.16–5.17, $\delta(H^{1,3})$ 5.43–5.51]. Bidentate coordination of dppf is evident from its single ^{31}P resonance in both **9** (δ = 54.9 ppm) and **10** (δ = 54.8 ppm). Monodentate coordination of the xanthate ligand was supported by X-ray diffraction analysis.

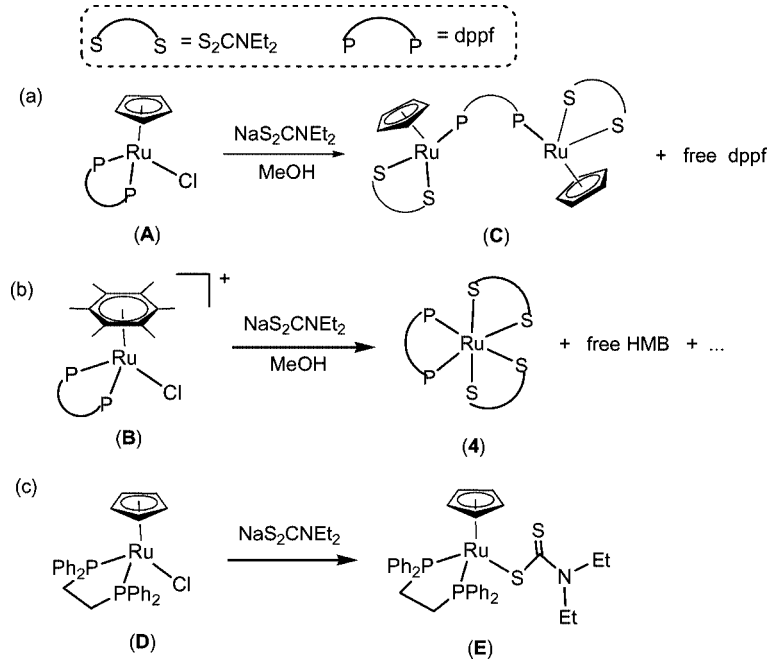

Scheme 4.[3a]

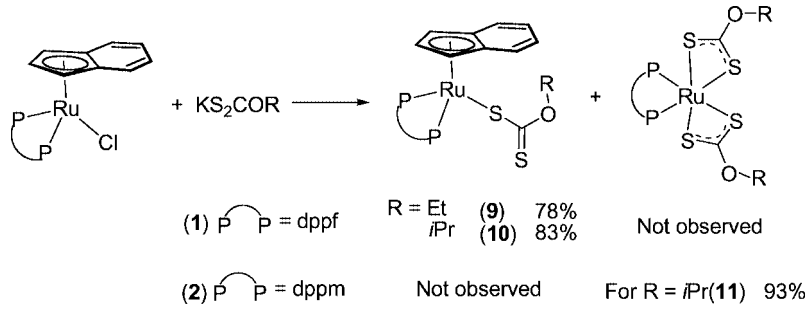

Scheme 5.

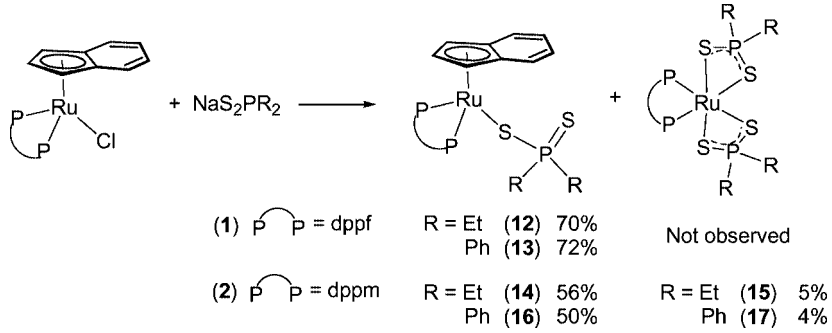

Scheme 6.

Complex **11** was formulated, based on its spectroscopic data. Its ^{1}H NMR spectrum showed the absence of a η^5-Ind ligand and its ^{31}P NMR spectrum showed a singlet at $\delta = 4.1$, assignable to chelating dppm. The FAB$^+$-mass spectrum showed the molecular ion peak at *m*/*z* 756, consistent with the presence of the non-indenyl six-coordinate complex.

Reaction with Dialkyl/Aryl Dithiophosphinates

The reactions of **1** with NaS_2PR_2 gave high yields of [(Ind)Ru(dppf)(η^1-S_2PR_2)] [R = Et (**12**), R = Ph (**13**)] (Scheme 6). The similar reaction of the dppm complex **2** gave the dppm analogues of **12** and **13**, viz. [(Ind)Ru(dppm)(η^1-S_2PR_2)] [R = Et (**14**), 56%; and R = Ph (**16**), 50%], the lower yields probably arising from degradation to the non-indenyl compounds, [Ru(dppm)(η^2-S_2PR_2)$_2$] [R = Et (**15**) and R = Ph (**17**)], which were isolated in 4–5% yields.

The ^{1}H NMR spectra of **12**–**14** and **16** showed η^5-Ind bonding to the Ru center, δ(H^2) 4.84–5.15 and δ(H^{1,3}) 5.34–6.12. In their ^{31}P NMR spectra, the chelating diphosphanes are seen as doublets (in the range $\delta = 53.1$–54.8 for η^2-dppf in **12** and **13**, and at $\delta = 12.5$–12.6 for η^2-dppm in **14** and **16**), while the monodentate dithiophosphinate ligand is seen as a triplet in the range $\delta = 84.9$–87.9 for S_2PEt_2 and $\delta = 70.9$–71.1 for S_2PPh_2.

The multiplet nature of these resonances is indicative of coupling between the two ligands in each of these complexes. However, for some unclear reason, such coupling is not evident in the ^{31}P NMR spectra of the non-indenyl complexes **15** and **17**, both of which show a singlet for the dithiophosphinate ligand at $\delta = 88.0$–105.6, as well as for dppm at $\delta = 4.0$–5.1.

Reactions of [(Ind)Ru(CO)$_2$I] (18) with NaS_2CNEt_2 and KS_2CO*i*Pr with or without Mediation by Trimethylamine *N*-Oxide

The reaction of **18** with ^-S_2CO*i*Pr in MeOH gave, within 30 min, free indene and the six-coordinate Ru complex, [Ru(η^2-S_2CO*i*Pr)$_2$(CO)$_2$] (**19**) (Scheme 7). It is apparent that the strong propensity of ^-S_2CO*i*Pr towards chelation facilitated the dissociation of the weaker indenyl ligand rather than the CO ligands. Liberation of free indene was likewise observed in the reactions of **18** with thiolates, for example, $^-$SMe or $^-S_2CNC_6H_4$.[13]

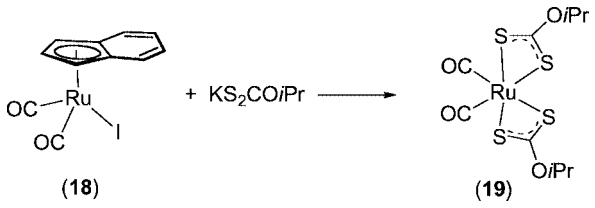

Scheme 7.

An attempt was made to hamper the dissociation of the indenyl ligand by generating a vacant site for coordination of the incoming bidentate thiolate. This was done by prior removal of CO ligands in **18** with trimethylamine *N*-oxide dihydrate, TMNO·2H$_2$O. It was found that decarbonylation of **18** resulted in a dark brown solution, from which a red

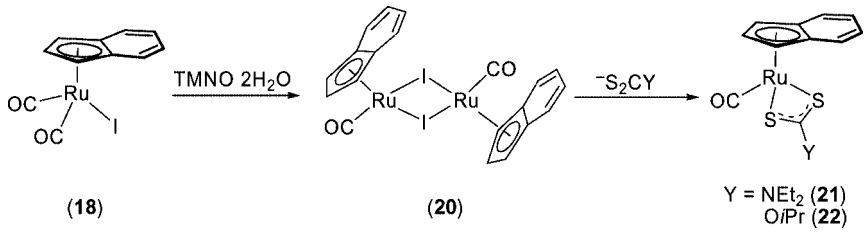

Scheme 8.

solid of $[(Ind)Ru(CO)(\mu\text{-}I)]_2$ (**20**) (70%) was obtained, undoubtedly from facile dimerization of the coordinatively unsaturated [(Ind)Ru(CO)I] species.

Complex **20** was characterized, based on its ^1H NMR spectrum, which showed η^5-Ind resonances at δ = 4.26 ($H^{1,3}$), 4.37 (H^2), and 6.54–7.59 (H^{5-8}), its ESI^+-mass spectrum, which gave the molecular ion peak at *m*/*z* 742.5 and an isotopic fragmentation pattern indicative of a Ru_2 moiety, and its IR spectrum, which showed a terminal CO stretch at 1925 cm^{-1}, in addition to an X-ray diffraction analysis.

The dark brown solution of **20** in CH_3CN reacted slowly with $^-S_2CNEt_2$ or ^-S_2CO*i*Pr giving dirty green and dirty yellow solutions, respectively, from which (Ind)Ru(CO){η^2-(S–S)} [S–S = S_2CNEt_2 (**21**, 55%), S_2CO*i*Pr (**22**, 81%)] was isolated (Scheme 8).

The infrared spectra of **21** and **22** in THF showed a new CO stretching frequency at 2031 and 2041 cm^{-1}, respectively. The presence of the η^5-Ind ligand was again indicated by the ^1H NMR signals at δ = 4.77–4.85 (H^2), 5.07–5.16 ($H^{1,3}$), and 6.83–7.16 (H^{5-8}). The molecular ions were observed at *m*/*z* 393 and 380, respectively. The structure of **21** has been determined by single-crystal X-ray diffraction analysis.

Crystallographic Studies

The molecular structure of **4a** is illustrated in the ORTEP diagram (Figure 1, with selected bond parameters), which shows Ru coordinated to η^5-Ind, η^2-S_2CNEt_2, and η^1-dppf ligands. The Cp rings of dppf are almost eclipsed (anticlinal) to each other, with a torsional angle (τ) of 136.58°. The slip-fold parameters of the indenyl ligand (see Table 1) suggest undistorted η^5-coordination,[14] with the benzenoid ring "flipped" towards the Ru center, probably a consequence of the relief in steric congestion around the metal center, which undoubtedly is the underlying cause for the dppf ligand to adopt a rare η^1-coordination mode, the first such case (as far as we are aware) in a structurally characterized mononuclear complex. Likewise steric demands have caused the pendant PPh_2 group to point away from the [(Ind)Ru(S_2CNEt_2)] fragment. The extensive electron delocalization in the S_2CNEt_2 ligand can be observed in the bond lengths of S1–C10, S2–C10, and C10–N1, the values of which lie between those of a single and a double bond (C–S 1.81 Å; C=S 1.61 Å; C–N 1.47 Å; C=N 1.27 Å).[15]

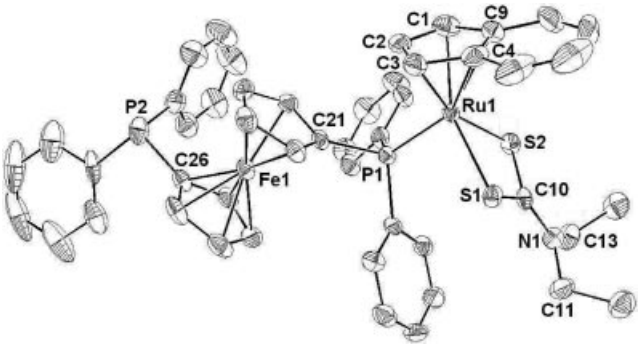

Figure 1. ORTEP diagram of **4a**. Thermal ellipsoids are drawn to 50% probability level. Hydrogen atoms are omitted for clarity. Selected bond lengths [Å] and angles [°]: Ru1–C* 1.873, Ru1–C1 2.180(5), Ru1–C2 2.159(5), Ru1–C3 2.185(5), Ru1–C4 2.309(5), Ru1–C9 2.302(5), Ru1–P1 2.2392(13), Ru1–S1 2.4068(13), Ru1–S2 2.3826(14), S1–C10 1.699(5), S2–C10 1.718(5), C10–N1 1.337(6), P1–C21 1.825(5), P2–C26 1.810(6), S1–Ru1–S2 71.85(4), S1–Ru1–P1 93.73(5), S2–Ru1–P1 88.04(5), S1–C10–S2 110.7(3), S1–C10–N1 126.3(4), S2–C10–N1 122.9(4), C10–N1–C11 121.1(4), C10–N1–C13 119.7(4), Ru1–P1–C21 111.90(16).

Table 1. Comparison of slip-fold parameters[a] of the (η^5-Ind)Ru complexes.

Complex	Δ [Å]	HA [°]	FA [°]
[(Ind)Ru(DTC_{Et})(η^1-dppf)] **4a**	0.123	4.68	3.53
[(Ind)Ru(dppf)(η^1-S_2COEt)] **9**	0.152	6.23	9.21
[(Ind)Ru(dppf)(η^1-S_2PEt_2)] **12**	0.203	7.52	12.91
[(Ind)Ru(dppm)(η^1-S_2PPh_2)] **16**	0.128	6.38	4.96
$[(Ind)Ru(CO)I]_2$ **20**	0.162, 0.185	6.32, 5.87	3.96, 4.18
[(Ind)Ru(CO)(DTC_{Et})] **21**	0.165	6.81	4.83
[(Ind)Ru(CO)I{$P(CH_2Ph)_3$}] **F**[17]	0.10	3.32	5.59
$[(Ind)RuH(PPh_3)_2]$ **G**[5a]	0.154	5.1	8.4

[a] Δ is the difference in the average bond lengths of the metal to the ring junction carbons, i.e., C4, C9, and of the metal to adjacent carbon atoms of the five-membered ring, i.e., C1, C3. HA is the angle between the planes defined by [C1,C2,C3] and [C1,C3,C4,C9]. FA is the angle between the planes defined by [C1,C2,C3] and [C4,C5,C6,C7,C8,C9][14] (see Figure 9 for atom numbering).

The asymmetric unit of complex **9** contains one ruthenium complex and two dichloromethane solvent molecules. The Ru center is coordinated to η^5-Ind, η^2-dppf, and a monodentate xanthate ligand. The Ru centers in **12** and **16** are similarly coordinated with a monodentate dithiophosphinate ligand. The ORTEP diagrams of complexes **9**, **12**, and **16** are shown in Figures 2, 3, and 4.

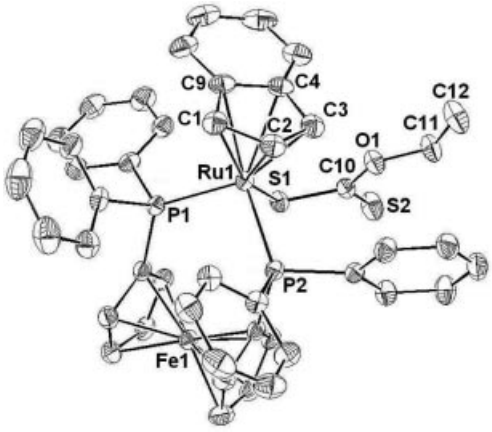

Figure 2. ORTEP diagram of **9**. Thermal ellipsoids are drawn to 50% probability level. Hydrogen atoms are omitted for clarity. Selected bond lengths [Å] and angles [°]: Ru1–C* 1.918, Ru1–C1 2.220(3), Ru1–C2 2.186(3), Ru1–C3 2.212(3), Ru1–C4 2.361(3), Ru1–C9 2.374(3), Ru1–P1 2.3110(7), Ru1–P2 2.2618(7), Ru1–S1 2.3964(7), S1–C10 1.712(3), S2–C10 1.674(3), C10–O1 1.331(4), P1–Ru1–P2 97.43(3), S1–Ru1–P1 89.31(3), S2–Ru1–P2 86.53(3), Ru1–S1–C10 116.03(10), S1–C10–S2 120.60(17), S1–C10–O1 116.4(2), S2–C10–O1 123.0(2), C10–O1–C11 118.5(2).

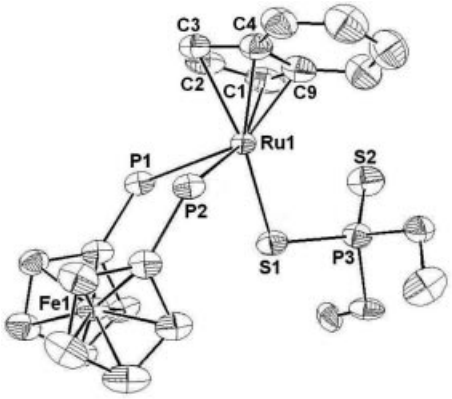

Figure 3. ORTEP diagram of **12**. Thermal ellipsoids are drawn to 50% probability level. Hydrogen atoms and phenyl groups are omitted for clarity. Selected bond lengths [Å] and angles [°]: Ru1–C* 1.941, Ru1–C1 2.244(8), Ru1–C2 2.168(7), Ru1–C3 2.182(7), Ru1–C4 2.408(7), Ru1–C9 2.424(8), Ru1–P1 2.2516(19), Ru1–P2 2.3181(18), Ru1–S1 2.4647(18), P1–Ru1–P2 98.98(7), S1–Ru1–P1 89.27(7), S1–Ru1–P2 86.07(6).

The η^5-indenyl ligands in **9** and **16** do not show noticeable distortion, while that of **12** is slightly distorted[14] (see Table 1). The fold angle of complex **16** indicates that the benzenoid ring of the indenyl ligand bends towards the ruthenium center rather than away as observed in **9** and **12**. This presumably is due to the coordination of a less sterically demanding dppm compared to dppf. Another interesting feature in the structures of complexes **9**, **12**, and **16** is the orientation of the monodentate dithiolate ligand. The noncoordinating S atom of the xanthate ligand in **9** is oriented away from the indenyl ligand, whereas those of the dithiophosphinate ligands in **12** and **16** are pointing towards the indenyl ligands, as shown in their stereo views. This probably arises from steric repulsion between the two

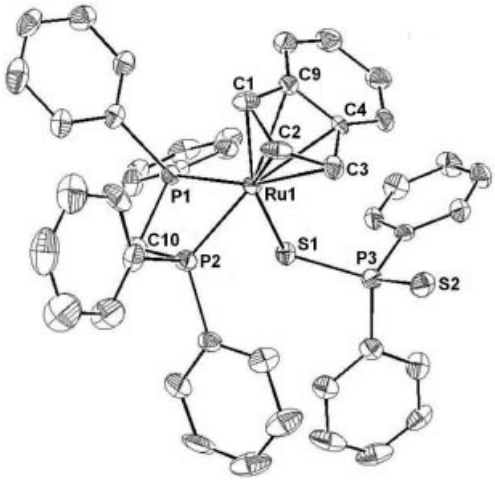

Figure 4. ORTEP diagram of **16**. Thermal ellipsoids are drawn to 50% probability level. Hydrogen atoms are omitted for clarity. Selected bond lengths [Å] and angles [°]: Ru1–C* 1.884, Ru1–C1 2.161(7), Ru1–C2 2.183(7), Ru1–C3 2.223(7), Ru1–C4 2.318(7), Ru1–C9 2.321(7), Ru1–P1 2.2695(19), Ru1–P2 2.242(2), Ru1–S1 2.439(2), S1–P3 2.044(3), S2–P3 1.965(3), C10–P1 1.848(7), C10–P2 1.848(8), P1–Ru1–P2 72.20(7), S1–Ru1–P1 84.98(7), S2–Ru1–P2 84.76(7), Ru1–S1–P3 117.45(10), S1–P3–S2 121.02(14), P1–C10–P2 92.0(3).

R groups in dithiophosphinate ligands and the indenyl ligands.

The six-coordinate complexes **7**, **11**, and **17** have also been characterized by X-ray diffraction analysis. Their molecular structures were found to be similar to those of known analogues, such as $[Ru(dppf)(S_2CNEt_2)_2]$[8] and $[Ru(L)(L')(S_2Z)_2]$ (L = CO, L = PEt_3, Z = $CNMe_2$, COEt, L = L′ = PMe_2Ph, Z = PEt_2)[16] (see electronic supporting information).

The molecular structure of the di-iodo-bridged complex **20** is shown in the ORTEP diagram (Figure 5). The structure exhibits crystallographic mirror symmetry, with the

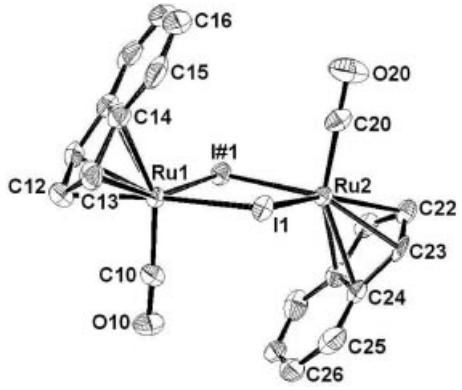

Figure 5. ORTEP drawing of $[(Ind)Ru(CO)I]_2$ **20** with 50% probability thermal ellipsoids. H atoms are omitted for clarity. Selected bond lengths [Å] and angles [°]: Ru1–C* 1.874, Ru1–C12 2.142(16), Ru1–C13 2.172(10), Ru1–C14 2.334(10), Ru2–C* 1.885, Ru2–C22 2.141(15), Ru2–C23 2.171(10), Ru2–C24 2.356(10), Ru1···Ru2 4.014, Ru1–I1 2.716(10), Ru2–I1 2.717(10), Ru1–C10 1.820(15), Ru2–C20 1.812(16), I1–Ru1–I#1 84.37(4), I1–Ru2–I#1 84.35(4), C10–Ru1–I1 93.1(4), C20–Ru2–I1 92.5(4), Ru1–I1–Ru2 95.26(3).

mirror plane passing through the two Ru centers, the two CO ligands and the center of the two η^5-Ind ligands through C12 and C22. As in $[(Ind)Ru(CO)_2]_2$, the structure possesses two *trans* CO ligands and two *trans* [(Ind)-Ru(CO)] fragments, but unlike it, there is no interaction between Ru1 and Ru2 (4.014 Å).

The ORTEP diagram for the molecular structure of **21** is depicted in Figure 6, together with selected bond parameters. The structure shows a three-legged piano-stool configuration at Ru^{II}, being coordinated to η^5-Ind, η^2-S_2CNEt_2, and one CO ligand. The slip-fold parameters for **21** are in agreement with η^5-coordination of Ind.[14] As in the structure of **4a**, the metric data show that there is extensive electron delocalization in the S_2CNEt_2 ligand.

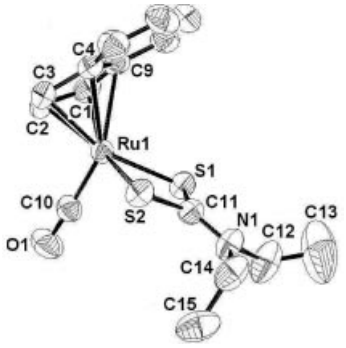

Figure 6. ORTEP drawing of $(Ind)Ru(CO)(S_2CNEt_2)$ **21** with 50% probability thermal ellipsoids. H atoms are omitted for clarity. Selected bond lengths [Å] and angles [°]: Ru1–C* 1.910, Ru1–C1 2.210(4), Ru1–C2 2.174(4), Ru1–C3 2.191(4), Ru1–C4 2.358(4), Ru1–C9 2.372(4), Ru1–S1 2.4035(10), Ru1–S2 2.3930(10), S1–C11 1.712(4), S2–C11 1.724(4), C11–N1 1.320(5), Ru1–C10 1.807(4), S1–Ru1–S2 72.22(3), S1–C11–S2 110.7(2).

An examination of slip-fold parameters of the indenyl complexes in this study and two other reported examples (Table 1) shows that complexes **4a**, **16**, **20**, and **21** possess FA values smaller than their HA values. This observation is unusual for η^5-indenyl complexes. The probable cause is the lack of a bulky ligand directly below the benzenoid ring of the Ind ligand in these complexes, unlike the structural feature found in **9**, **12**, **F**, and **G**. In these four latter phosphane complexes, the steric repulsion between the indenyl and bulky phosphane ligands forces the benzenoid ring to "flip" away from the Ru center, hence resulting in greater FA values.

Lability of the Indenyl Ligand

The foregoing results indicate that the lability of the indenyl ligand is influenced by the incoming 1,1-dithiolate and the coligands, according to the following trends: (i) dithiolates: $^-S_2CNR_2 > {}^-S_2COR > {}^-S_2PR_2$, (ii) coligands: CO ≈ dppm > dppf. Trend (i) can be readily rationalized, based on e-density considerations of the S donor atoms. The observation of monodenticity of the S_2PR_2 moiety in the high-yield indenyl complexes, **12**–**14** and **16**, is significant. In this dithiolate series, the S atoms in $^-S_2PR_2$ possess the most *localized* and hence highest electron density, whereas those in $^-S_2CNR_2$ possess the *lowest* electron density because of extensive electron delocalization. Hence the increased tendency of the latter towards chelation. In the absence of a vacant site or an easily displaceable ligand, chelation of a ligand will inevitably enforce dissociation of the indenyl ligand. For rationalizing trend (ii), we note that the benzenoid ring of the indenyl ligand can be considered as an electron-withdrawing group,[18] hence an electron-rich Ru center is required for strong interaction with η^5-Ind through its fused C_5H_3 ring, a situation provided by strong donor coligands like dppf, while labilization of the indenyl ligand will be assisted by the presence of a strong π-acceptor coligand, like CO.

The application of density functional theory has provided an understanding of the effect of different ligands on the energetics of $\eta^5 \rightarrow \eta^3$ ring slippage of the indenyl ligand and hence on its dissociation tendency. In a recent study, Veiros et al. demonstrated that the effect of the nature of the coligands on the strength of the indenyl–metal bond plays an important role in the energetics of η^5 versus η^3 indenyl–molybdenum complexes.[19] Because of the constraints on computational time, we have selected the complexes $[(Ind)Ru(L)_2(S_2COMe)]$ (**H1**: L = $PMeH_2$, **H2**: L = PH_3, **H3**: L = CO), containing small phosphane ligands such as PH_3 and PH_2Me, rather than the larger diphos ligands (dppm or dppf), as the model compounds for study. In this series, complex **H1** contains the strongest σ-donor ligand, followed by **H2**, with **H3** possessing the strongest π-acceptor ligand. The dissociation of the indenyl ligand by $\eta^5 \rightarrow \eta^3 \rightarrow \eta^1$ has been considered and the results are presented in Figure 7.

It was found that $\eta^5 \rightarrow \eta^3$ indenyl ring slippage in complexes **H1** and **H2** possesses comparable activation energy (67 and 70 kJ/mol, respectively), with the process in **H1** being slightly more endothermic (7.4 kJ/mol). However, a remarkable difference was observed in the case of the strong π-acceptor CO in complex **H3**. Not only is the activation energy of the slippage almost half that for both **H1** and **H2** (33 kJ/mol), but the η^3-Ind coordination mode is more favorable, with the $\eta^5 \rightarrow \eta^3$ ring slippage process being exothermic (–13 kJ/mol). This is consistent with the expectation that stronger σ-donor ligands enhance the interaction between electron-rich Ru and the η^5-Ind ligand and vice versa. Therefore, as the dithiolate ligand tends to chelate to the electron-deficient Ru, the weak interaction of the η^5-Ind ligand and the Ru center would have facilitated the ease of $\eta^5 \rightarrow \eta^3$ slippage, and the combined effect would be the dissociation of the indenyl ligand.

A comparison between the effect of xanthate and dithiocarbamate ligands on indenyl ring slippage has also been made using the PH_3-containing complex **H4** as the model compound. As shown in Figure 1, the formation of the η^3-Ind isomer of the dithiocarbamate complex **H4** is a much more exothermic process. Unfortunately the transition state for this process could not be located, though it is not uncommon for activation energies of highly exothermic processes to be much lower or even close to zero, thus causing the transition state to assume a structure similar to that of

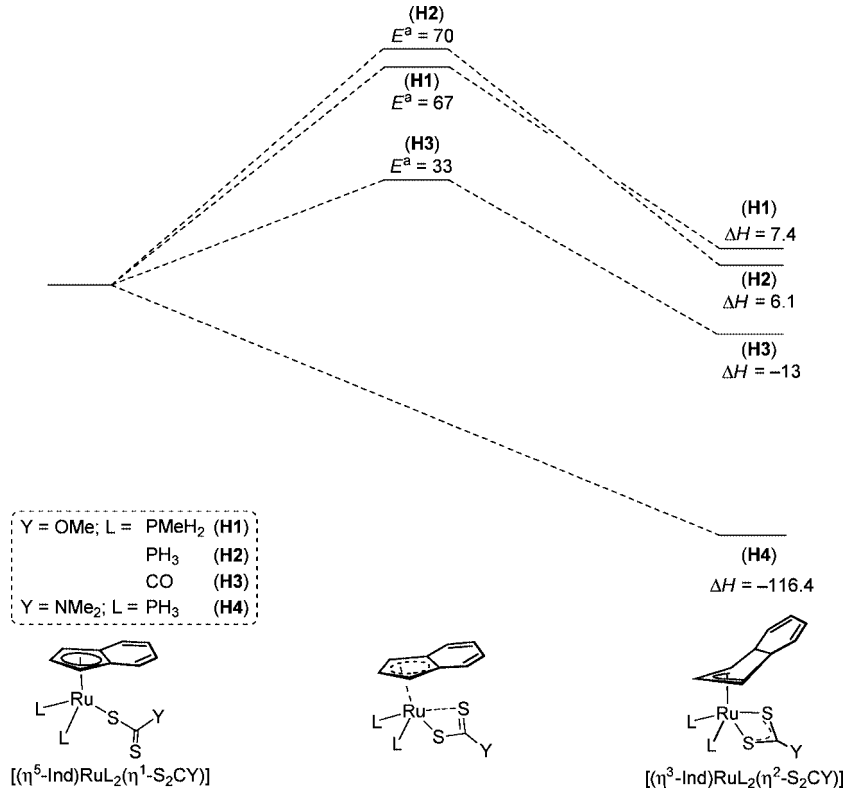

Figure 7. Energy diagram of ring slippage from $\eta^5 \rightarrow \eta^3$ (E^a is activation energy in kJ/mol).

the reactant. This may have caused difficulty in optimizing the transition-state structure using computational methods. Nevertheless the calculations indicated that $^-S_2CNR_2$ exerts a stronger effect than xanthate in causing indenyl ring slippage, in good agreement with the trend observed in the experimental data.

Electrochemical Studies

Cyclic voltammograms performed at a GC electrode in 0.5 mM solutions of **10** and **13** in CH_2Cl_2 at 233 K are shown in Figure 8. Complex **10** displayed one chemically irreversible oxidation process at about 0 V versus Fc/Fc^+. The expression "chemical reversibility" when used in connection with cyclic voltammetry experiments relates to the ratio of the oxidative (i_p^{ox}) to reductive peak currents (i_p^{red}). The i_p^{ox}/i_p^{red} ratio approaches unity for a fully chemically reversible process. Complex **13** showed three oxidation processes, although the two most positive processes displayed small reverse peaks when the scan direction was reversed, suggesting instability of the highly oxidized states. Increasing the scan rate up to 5 V/s did not improve the chemical reversibility of the processes shown in Figure 8. Table 2 lists the reversible oxidation potentials ($E^r_{1/2}$) that were calculated from CV data under conditions where the i_p^{ox}/i_p^{red} ratio was equal to unity and using the relationship [Equation (1)]

$$E^r_{1/2} = (E_p^{ox} + E_p^{red})/2 \quad (1)$$

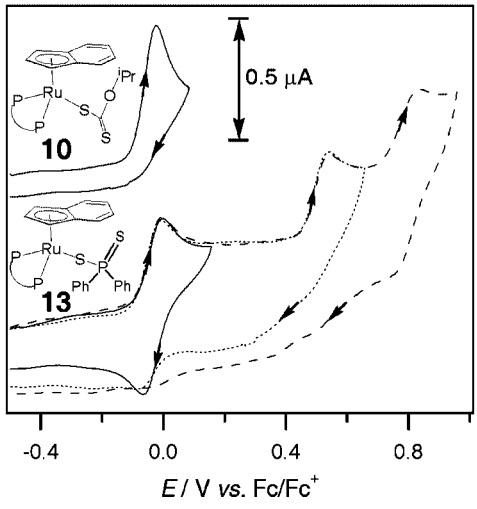

Figure 8. Cyclic voltammograms performed at a 1-mm diameter planar GC electrode in CH_2Cl_2 (0.25 M Bu_4NPF_6) at 233 K at a scan rate of 100 mV/s for 0.5 mM **10** and **13**.

where E_p^{ox} and E_p^{red} are the anodic and cathodic peak potentials respectively. In situations where small reverse peaks were observed, only the forward (oxidative) peak potentials are given.

The peak current intensities were similar to those obtained under identical conditions for the one-electron oxidation of **1**, [(Ind)Ru(dppf)(SMe)], [(Ind)Ru(dppf)(SPh)],[7]

Table 2. Cyclic voltammetric data obtained at a scan rate of 100 mV/s at a 1-mm diameter glassy carbon electrode at 233 K in CH_2Cl_2 with 0.25 M Bu_4NPF_6 as the supporting electrolyte.

Compound	Oxidation process[a]			
	E_p^{ox} [V][b]	E_p^{red} [V][c]	$E^r_{1/2}$ [V][d]	ΔE [mV][e]
10	–0.023			
13	–0.004	–0.068	–0.04	64
	+0.540			
	+0.830			

[a] All potentials in Table 2 are relative to the ferrocene/ferrocenium redox couple. [b] E_p^{ox} is the oxidative peak potential. [c] E_p^{red} is the reductive peak potential. [d] $E^r_{1/2} = (E_p^{red} + E_p^{ox})/2$. [e] $\Delta E = |E_p^{ox} - E_p^{red}|$.

I, and [Cp*Ru(dppf)Cl] (**VI**), indicating that **10** and **13** were also oxidized by one electron. However, **1**, [(Ind)Ru(dppf)(SMe)], [(Ind)Ru(dppf)(SPh)], **I**, and **VI** showed two or three one-electron chemically reversible oxidation processes, whilst cyclic voltammograms performed on solutions of **10** and **13** indicated that their oxidized states were relatively unstable even at low temperatures (Figure 8).[7]

Based on previous studies, it is thought that the initial oxidation process in Figure 8 for **10** and **13** is associated with Ru^{II} being oxidized to Ru^{III} (rather than oxidation in the region of dppf), as this process is very sensitive to the substituent (S or Ind) coordinated to the Ru. It is thought that the second process in the CV of **13** is associated with oxidation in the region of dppf, as the potential is close to that observed in other dppf-containing complexes,[7] while the third oxidation process is associated with further oxidation of the Ru ion. This would explain why the third oxidation process shows more chemical reversibility than the second process, if the individual regions (Ru and Fe) are not electronically communicating, then it is possible that the individual oxidation processes are semi-independent of one another (i.e., the first and third are associated with oxidation of the Ru ion, whilst the second process involves oxidation in the vicinity of dppf).

Both compounds displayed one chemically irreversible reduction process at very negative potentials (about –2.5 V vs. Fc/Fc^+), with a similar current magnitude to the first oxidation process (indicating that the same number of electrons were transferred). It is not possible to conclude whether the chemical instability of the reduced compounds is because of increased chemical reactivity due to the very high reduction potentials, or due to an $\eta^5 \rightarrow \eta^3$ ring slippage mechanism following reduction.

Conclusions

The lability of the Ind ligand in halide substitution of [(Ind)Ru(L_2)Cl] [L_2 = dppf, dppm or $(CO)_2$] with 1,1′-dithiolates is dependent on several variables: (i) the nature of the coligand L_2, which follows a lability order: dppf < dppm ≈ CO, in agreement with the electron donor capability of L_2 and calculated energetics for $\eta^5 \rightarrow \eta^3$ ring slippage in related (Ind)Ru complexes, (ii) the incoming dithiolates, which results in ease of indenyl ligand dissociation at (Ind)Ru(dppf) as follows: dithiocarbamates > xanthates > dithiophosphinates, in agreement with DFT calculations, and (iii) the solvent medium, as illustrated in complete dissociation of Ind from (Ind)Ru(dppf) in dithiocarbamate substitution in the highly polar solvent MeOH relative to partial dissociation in CH_2Cl_2. In the case of the (Ind)-$Ru(CO)_2$ substrate, dissociation of Ind could be averted by chemically assisted decarbonylation of the complex before reaction with 1,1-dithiolate ligands. The hydride species [(Ind)Ru(diphos)H], formed in solvent- and stoichiometry-dependent yields in the (diphos) systems, presumably arose from the presence of OMe^- in MeOH, as previously observed.[7] Cyclic voltammetry experiments indicate that the (Ind)Ru(dppf) derivatives containing η^1-S_2CO*i*Pr and η^1-S_2PPh_2 can be oxidized in one-electron chemical irreversible and reversible processes, respectively, at a scan rate of 100 mV/s at about 0 V versus Fc/Fc^+.

Experimental Section

General: All reactions were carried out using conventional Schlenk techniques under inert nitrogen or under argon in an M. Braun Labmaster 130 Inert Gas System. NMR spectra were measured on a Bruker 300 FT NMR spectrometer, ^1H chemical shifts were referenced to residual solvent in the deuterio-solvents, C_6D_6 or CD_3CN, and ^{31}P chemical shifts were referenced to external H_3PO_4. IR spectra in KBr pellets were measured in the range 4000–400 cm^{-1} by means of a BioRad FTS-165 FTIR instrument. Mass spectra were run on a Finnigan Mat 95XL-T (FAB) or a Finnigan-MAT LCQ (ESI) spectrometer. Voltammetric experiments were conducted with a computer-controlled Eco Chemie μAutolab III potentiostat. The electrochemical cell was jacketed in a glass sleeve and cooled to 233 K using a Lauda RL6 variable-temperature methanol-circulating bath. Elemental analyses were performed by the microanalytical laboratory in-house. [(Ind)Ru(dppf)Cl] (**1**),[20] [(Ind)Ru(dppm)Cl] (**2**),[21] and [(Ind)Ru$(CO)_2$I] (**18**)[22] were prepared by published methods. All other chemicals were obtained commercially and used without any further purification. All solvents were dried with sodium/benzophenone and distilled before use. Celite (Fluka AG) and silica gel (Merck Kieselgel 60, 230–400 Mesh) were dried at 140 °C overnight before chromatographic use.

Conventional numbering of indenyl protons shown in Figure 9 is followed in the assignment of NMR signals.

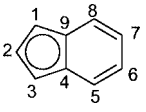

Figure 9. Atom labeling of the indenyl ligand.

(I) Reactions of (Ind)Ru(diphosphane) Complexes

(a) Reactions with Dialkyl Dithiocarbamates

(i) Reactions of [(Ind)Ru(dppf)Cl] (**1**) with NaS_2CNR_2 were carried out at stoichiometries of 1:1 and 1:4. A typical reaction for each stoichiometry is described for R = Et, as follows:

1:S_2CNR_2 (1:1): $NaS_2CNEt_2 \cdot 3H_2O$ (10 mg, 0.04 mmol) was added to a suspension of **1** (35 mg, 0.04 mmol) in MeOH (5 mL) and the mixture was stirred at room temp. for 18 h. The color of the suspen-

sion slowly changed from red to yellow. The suspension was filtered and the residue was extracted using toluene (2 × 5 mL). The filtrate was examined by GC/MS, which showed indene. The extract was concentrated to about 2 mL and loaded onto a silica gel column (2 × 5 cm) prepared in n-hexane. Elution gave two fractions: (i) a yellow eluate in toluene (8 mL), which yielded [(Ind)Ru(dppf)H] (**6**) (13 mg, 39% yield) (for the reaction in which R = Me, 11 mg, 32% yield, R = C_5H_{10}, 8 mg, 25% yield), (ii) a yellow eluate in toluene/THF (1:1, 10 mL), which yielded [Ru(η^2-dppf)(η^2-S_2CNEt_2)$_2$] **4** (25 mg, 60% yield). Similar reactions gave **3** (R = Me), 22 mg, 56% yield, and **5** (R = C_5H_{10}), 25 mg, 58% yield. Analytical pure samples of complexes **3**–**5** were obtained by recrystallization from THF/hexane (1:5).

1:S_2CNR_2 (1:4). Reaction in MeOH: $NaS_2CNEt_2 \cdot 3H_2O$ (40 mg, 0.16 mmol) was added to a suspension of **1** (35 mg, 0.04 mmol) in MeOH (5 mL) and the mixture was stirred at room temp. for 18 h. The color of the suspension slowly changed from red to yellow. The solvent was removed in vacuo and the residue was extracted with toluene (2 × 5 mL). The extract was concentrated to about 2 mL, addition of hexane (2 mL) at –30 °C for 1 d gave yellow crystals of **4** (37 mg, 90% yield). Similar reactions gave **3** (R = Me), 36 mg, 92% yield, and **5** (R = C_5H_{10}), 41 mg, 98% yield.

Reaction in CH_2Cl_2: $NaS_2CNEt_2 \cdot 3H_2O$ (60 mg, 0.24 mmol) was added to a solution of **1** (50 mg, 0.06 mmol) in CH_2Cl_2 (10 mL) and the mixture was refluxed for 4 h. The solution was evacuated to dryness and the residue extracted with diethyl ether (2 × 3 mL). The extract was concentrated to about 3 mL and kept at –30 °C, after 2 d, yellow microcrystals of **4** (16 mg, 28% yield) were collected. Addition of hexane (about 0.5 mL) to the mother liquor led to the isolation of red microcrystals of [(Ind)Ru(η^1-dppf)(η^2-S_2CNEt_2)] (**4a**) (20 mg, 36% yield) after two more days at –30 °C.

A small-scale reaction was carried out at stoichiometry 1:2, using **1** (5 mg, 6.2 μmol) and $NaS_2CNEt_2 \cdot 3H_2O$ (3 mg, 12 μmol) in MeOH (2 mL) and the red suspension was stirred at room temp. for 18 h. The resultant yellow suspension was filtered to give yellow solids, **4** (5 mg, 85% yield), and pale yellow filtrate. The ^{1}H and ^{31}P NMR spectra of the yellow solids (in C_6D_6) showed **4** as the sole product. A new batch of **1** (5 mg, 6.2 μmol) was added to the filtrate and the red suspension was stirred for another 18 h. The resultant yellow suspension was filtered and the yellow solids, **6** (4 mg, 84% yield) were obtained. The ^{1}H and ^{31}P NMR spectra of the yellow solids in C_6D_6 indicate the sole presence of **6**.

Data for 3: ^{1}H NMR (C_6D_6): δ = 2.41 and 2.43 [each s, 3 H, $S_2CN(CH_3)_2$], 3.94, 4.04, 4.62 and 4.69 (each s, 2 H, C_5H_4), 7.03–7.11, 7.21–7.25, 7.95 and 8.20–8.25 (m, 20 H, Ph) ppm. ^{31}P{^{1}H} NMR (C_6D_6): δ = 47.9 (s, dppf) ppm. IR (KBr): $\tilde{\nu}$ = 3053 (w), 2922 (w), 2855 (w), 1509 [m, SC(S)], 1432 [m, SC(S)], 1386 [s, SC(S)], 1262 [m, SC(S)], 1146 (m), 1086 (m), 1028 (m), 811 (w), 746 (w), 697 (m), 548 (w), 521 (w) cm^{-1}. FAB$^+$-MS: *m*/*z* (%) = 896 [M]$^+$, 776 [M – S_2CNMe_2]$^+$. $C_{40}H_{40}FeN_2P_2RuS_4 \cdot 1/4C_6H_{12}$ (917.39): calcd. C 54.3, H 4.7, N 3.1, S 14.0, found C 54.1, H 5.1, N 3.2, S 13.5.

Data for 4a: ^{1}H NMR (C_6D_6): δ = 0.61 [t, $^3J_{HH}$ = 7.4 Hz, 6 H, $S_2CN(CH_2CH_3)_2$], 2.81 and 3.04 [each m, $^3J_{HH}$ = 7.4 Hz, 2 H, $S_2CN(CH_2CH_3)_2$], 4.11 and 4.33 (each s, 2 H, C_5H_4), 4.19 (s, 4 H, C_5H_4), 4.56 (t, $^3J_{HH}$ = 2.5 Hz, 1 H, H^2), 4.89 (d, $^3J_{HH}$ = 2.5 Hz, 2 H, H^{1,3}), 7.04–7.16, 7.37–7.40, 7.42–7.48 and 7.75–7.81 (each m, total 24 H, H$^{5-8}$ and Ph) ppm. ^{31}P{^{1}H} NMR (C_6D_6): δ = 57.3 and –17.7 (each s, dppf) ppm. IR (KBr): $\tilde{\nu}$ = 3050 (w), 2972 (w), 2929 (w), 1484 [s, SC(S)], 1431 [vs, SC(S)], 1380 (w), 1324 (w), 1270 [m, SC(S)], 1215 (w), 1159 (m), 1092 (m), 1030 (m), 830 (w), 743 (m), 696 (vs), 543 (m), 517 (m) cm^{-1}. FAB$^+$-MS: *m*/*z* (%) = 804 [M – Ind]$^+$. $C_{48}H_{45}FeNP_2RuS_2$ (918.87): calcd. C 62.7, H 4.9, N 1.5, S 7.0, found C 62.6, H 5.2, N 1.3, S 6.9.

Data for 5: ^{1}H NMR (C_6D_6): δ = 0.95 (br. s, 12 H, $S_2CNC_5H_{10}$), 3.02, 3.63 (each br. s, 4 H, $S_2CNC_5H_{10}$), 3.95, 4.05, 4.62 and 4.71 (each s, 2 H, C_5H_4), 7.00–7.23, 7.69–7.72, 8.03–8.05 and 8.19–8.24 (each m, total 20 H, Ph) ppm. ^{31}P{^{1}H} NMR (C_6D_6): δ = 47.6 (s, dppf) ppm. IR (KBr): $\tilde{\nu}$ = 3048 (w), 2931 (m), 2853 (m), 1479 [s, SC(S)], 1433 [s, SC(S)], 1233 [s, SC(S)], 1129 (m), 1086 (m), 995 (m), 885 (w), 850 (w), 811 (w), 743 (m), 695 (s), 546 (m), 518 (m) cm^{-1}. FAB$^+$-MS: *m*/*z* (%) = 976 [M]$^+$, 816 [M – $S_2CNC_5H_{10}$]$^+$. $C_{46}H_{48}FeN_2P_2RuS_4$ (976.01): calcd. C 56.6, H 5.0, N 2.9, S 13.1, found C 56.5, H 5.0, N 2.7, S 12.9.

(ii) Reactions of [(Ind)Ru(dppm)Cl] **2** with NaS_2CNEt_2 were carried out at stoichiometries of 1:1 and 1:4.

2:S_2CNR_2 (1:1): $NaS_2CNEt_2 \cdot 3H_2O$ (10 mg, 0.04 mmol) was treated with **2** (20 mg, 0.04 mmol) in MeOH (5 mL). A similar workup as described above for the dppf analogue yielded [Ru(dppm)(η^2-S_2CNEt_2)$_2$] (**7**) (18 mg, 58% yield) and [(Ind)Ru(dppm)H] (**8**) (5 mg, 20% yield), identified by its published proton NMR spectroscopic data, notably δ(H) –14.21 (s) in C_6D_6 versus the lit. value of –14.12 (s) in CD_2Cl_2.[10]

Using 2:S_2CNR_2 (1:4): A similar reaction as described above for **1** was carried out, using $NaS_2CNEt_2 \cdot 3H_2O$ (20 mg, 0.08 mmol) and [(Ind)Ru(dppm)Cl] (**2**) (10 mg, 0.02 mmol) in MeOH (5 mL) and the mixture was stirred for 4 h. Similar workup procedures gave yellow crystals of [Ru(dppm)(η^2-S_2CNEt_2)$_2$] (**7**) (10 mg, 81% yield).

Data for 7: ^{1}H NMR (C_6D_6): δ = 0.63–0.68 and 0.86–0.91 (each t-like m, 6 H, CH_3), 2.85–3.02 (m, 2 H, CH_2CH_3), 3.15–3.28 (m, 2 H, CH_2CH_3), 3.43–3.62 (m, 4 H, CH_2CH_3), 4.73 (t, $^2J_{HP}$ = 9.9 Hz, 2 H, CH_2 of d), 6.98–7.16 (m, 14 H, Ph), 7.54–7.58 (m, 3 H, Ph), 7.93–7.95 (m, 3 H, Ph) ppm. ^{31}P{^{1}H} NMR (C_6D_6): δ = 3.7 (s, dppm) ppm. IR (KBr): $\tilde{\nu}$ = 3050 (w), 2974 (w), 2929 (w), 2871 (w), 1483 [s, SC(S)], 1426 [s, SC(S)], 1303 (w), 1268 [s, SC(S)], 1214 (m), 1142 (m), 1091 (m), 997 (w), 911 (w), 848 (w), 698 (s), 535 (m) cm^{-1}. FAB$^+$-MS: *m*/*z* (%) 782 [M]$^+$, 634 [M – S_2CNEt_2]$^+$. $C_{35}H_{42}N_2P_2RuS_4$ (782.00): calcd. C 53.8, H 5.4, N 3.6, S 16.4, found C 53.8, H 5.5, N 3.7, S 16.2.

(b) Reactions with Alkyl Xanthates

(i) KS_2COR (0.07 mmol, R = Et, 11 mg, R = *i*Pr, 12 mg) was added into a solution of **1** (15 mg, 0.02 mmol) in CH_2Cl_2 (10 mL) and the mixture was refluxed. The reaction was not accompanied by any color change, hence it was monitored by ^{1}H and ^{31}P NMR spectroscopy. After the reaction was complete (about 4 h), the solution was evacuated to dryness. The solid residue was extracted with toluene (2 × 2 mL) and the concentrated extract recrystallized from 1:2 THF/hexane at –30 °C. Red microcrystals of [(Ind)Ru(dppf)(η^1-S_2COR)] [R = Et (**9**), 13 mg, 78% yield, R = *i*Pr (**10**), 14 mg, 83% yield] were obtained after one day.

Data for 9: ^{1}H NMR (C_6D_6): δ = 1.06 (t, $^3J_{HH}$ = 7.4 Hz, 3 H, $S_2COCH_2CH_3$), 3.55, 3.81, 3.98 and 4.34 (each s, 2 H, C_5H_4), 4.41 (q, $^3J_{HH}$ = 7.4 Hz, 2 H, $S_2COCH_2CH_3$), 5.16 (s, 1 H, H^2), 5.43 (s, 2 H, H^{1,3}), 6.98–7.14, 7.26–7.30 and 7.43–7.48 (each m, total 24 H, H$^{5-8}$ and Ph) ppm. ^{31}P{^{1}H} NMR (C_6D_6): δ = 54.9 (s, dppf) ppm. IR (KBr): $\tilde{\nu}$ = 3050 (w), 2978 (w), 1478 (w), 1432 (w), 1382 (w), 1165 [s, (CO)], 1105 [s, (CS)], 1030 [vs, (CS)], 858 w, 819 w, 792 w, 744 m, 697 s, 631 w, 513 m. FAB$^+$-MS: *m*/*z* (%) = 892 [M]$^+$, 777 [M – Ind]$^+$, 655 [M – Ind – S_2COEt]$^+$. $C_{46}H_{40}FeOP_2RuS_2$ (891.80): calcd. C 62.0, H 4.5, S 7.2, found C 61.6, H 4.8, S 7.5.

Data for 10: ^{1}H NMR (C_6D_6): δ = 1.25 [d, $^3J_{HH}$ = 5.76 Hz, 6 H, $S_2COCH(CH_3)_2$], 3.55, 3.84, 3.98 and 4.46 (each s, 2 H, C_5H_4),

5.17 (s, 1 H, H^2), 5.51 (s, 2 H, $H^{1,3}$), 5.67 [sept, J = 6.6 Hz, 1 H, $S_2COCH(CH_3)_2$] 7.00–7.47 (m, 24 H, H^{5-8} and Ph) ppm. $^{31}P\{^1H\}$ NMR (C_6D_6): δ = 54.8 (s, dppf) ppm. IR (KBr): $\tilde{\nu}$ = 3047 (w), 2963 (w), 2923 (w), 1940 (w), 1478 (w), 1433 (w), 1382 (w), 1261 [m, (CO)], 1187 (w), 1089 [s, SC(S)], 1015 [s, SC(S)], 803 (s), 743 (m), 695 (s), 631 (w), 507 (m) cm^{-1}. FAB^+-MS: m/z (%) = 906 $[M]^+$, 791 $[M - Ind]^+$, 771 $[M - S_2CO{i}Pr]^+$, 655 $[M - Ind - S_2CO{i}Pr]^+$. $C_{47}H_{42}FeOP_2RuS_2$ (905.83): calcd. C 62.3, H 4.7, S 7.0, found C 61.9, H 4.8, S 6.6.

(ii) $KS_2CO{i}Pr$ (23 mg, 0.13 mmol) was added to a solution of **2** (20 mg, 0.03 mmol) in MeOH (5 mL) and the solution was stirred at room temp. for 18 h. The color of the solution changed slowly from red to yellow in the course of reaction. The yellow product solution was evacuated to dryness and the residue extracted with toluene (2 × 2 mL). Addition of hexane (about 4 mL) into the concentrated extract (about 2 mL) at –30 °C for 1 d gave [Ru(dppm)(η^2-$S_2CO{i}Pr$)$_2$] (**11**) (27 mg, 93% yield) as yellow microcrystals.

Data for 11: ^1H NMR (C_6D_6): δ = 0.87–0.89 and 0.95–0.97 (each d-like m, 6 H, CH_3), 4.67 (t, $^2J_{HP}$ = 9.9 Hz, 2 H, CH_2 of d), 5.34 [sept, $^3J_{HH}$ = 6.6 Hz, 2 H, $CH(CH_3)_2$], 6.95–7.02 (m, 7 H, Ph), 7.08–7.16 (m, 5 H, Ph), 7.38–7.45 (m, 4 H, Ph), 7.81–7.89 (m, 4 H, Ph) ppm. $^{31}P\{^1H\}$ NMR (C_6D_6): δ = 4.1 (s, dppm) ppm. IR (KBr): $\tilde{\nu}$ = 3049 (w), 2976 (w), 2930 (w), 1481 (w), 1432 (m), 1371 (w), 1231 [vs, (CO)], 1093 [vs, SC(S)], 1033 [s, SC(S)], 905 m, 723 s, 696 s, 538 m, 509 s. FAB^+-MS: m/z (%) = 756 $[M]^+$. $C_{33}H_{36}O_2P_2RuS_4$ (755.92): calcd. C 52.4, H 4.8, S 17.0, found C 52.4, H 4.8, S 17.0.

(c) Reactions with Dithiophosphinates

(i) NaS_2PR_2 (0.04 mmol, R = Et, 7 mg, R = Ph, 11 mg) was added to a suspension of **1** (10 mg, 0.01 mmol) in MeOH and the mixture was stirred at room temp. for 18 h. The resultant red solution was evacuated to dryness and the residue extracted with toluene (2 × 3 mL). The extract was concentrated to about 2 mL and loaded on a silica gel column (1.5 × 2.0 cm). Elution with 2:1 hexane/diethyl ether (3–5 mL) and subsequent workup gave red crystals of [(Ind)Ru(dppf)(η^1-S_2PR_2)] (R = Et (**12**), 8 mg, 70% yield, R = Ph (**13**), 9 mg, 72% yield).

Data for 12: ^1H NMR (C_6D_6): δ = 1.18–1.30 [m, 6 H, $S_2P(CH_2CH_3)_2$], 1.90–2.12 [m, 4 H, $S_2P(CH_2CH_3)_2$], 3.70, 3.81, 4.20 and 5.15 (each s, 2 H, C_5H_4), 4.84 (s, 1 H, H^2), 5.70 (s, 2 H, $H^{1,3}$), 6.90–6.93 and 7.58–7.61 (each 4-line m, $^3J_{HH}$ = 3.3 Hz, 2 H, H^{5-8}), 7.11–7.68 (m, 20 H, Ph) ppm. $^{31}P\{^1H\}$ NMR (C_6D_6): δ = 54.8 (d, $^3J_{PP}$ = 16 Hz, dppf), 87.5 (t, $^3J_{PP}$ = 16 Hz, S_2PEt_2) ppm. IR (KBr): $\tilde{\nu}$ = 3054 (w), 2966 (w), 2924 (w), 2868 (w), 1479 (w), 1433 (m), 1325 (w), 1157 (w), 1090 (m), 1030 (m), 821 (m), 746 [s, (PS)], 695 (PS), 594 [w, (PS)], 632 (m), 511 (s) cm^{-1}. FAB^+-MS: m/z (%) = 924 $[M]^+$, 809 $[M - Ind]^+$, 771 $[M - S_2PEt_2]^+$, 655 $[M - Ind - S_2PEt_2]^+$. $C_{47}H_{45}FeP_3RuS_2$ (923.833): calcd. C 61.1, H 4.9, found C 61.4, H 4.7.

Data for 13: ^1H NMR (C_6D_6): δ = 3.60, 3.79, 4.05 and 5.20 (each s, 2 H, C_5H_4), 5.10 (s, 1 H, H^2), 5.34 (s, 2 H, $H^{1,3}$), 6.61–6.64 and 7.35–7.39 (each 4-line m, 2 H, H^{5-8}), 7.05–7.19, 7.26–7.33 and 7.45–7.51 (each m, total 26 H, Ph), 8.43–8.50 (4-line m, 4 H, Ph) ppm. $^{31}P\{^1H\}$ NMR (C_6D_6): δ = 53.1 (d, $^3J_{PP}$ = 15 Hz, dppf), 71.1 (t, $^3J_{PP}$ = 15 Hz, S_2PPh_2) ppm. IR (KBr): $\tilde{\nu}$ = 3052 (w), 2922 (w), 2854 (w), 1650 (w), 1477 (w), 1433 (m), 1158 (w), 1089 (m), 1033 (w), 821 (w), 745 [m, (PS)], 698 [s, (PS)], 649 [m, (PS)], 512 (m) cm^{-1}. FAB^+-MS: m/z (%) = 1020 $[M]^+$, 905 $[M - Ind]^+$, 771 $[M - S_2PPh_2]^+$, 655 $[M - Ind - S_2PPh_2]^+$. $C_{55}H_{45}FeP_3RuS_2$ (1019.91): calcd. C 64.8, H 4.5, S 6.3, found C 64.8, H 4.4, S 5.8.

(ii) NaS_2PR_2 (0.31 mmol, R = Et, 55 mg, R = Ph, 85 mg) was added to a suspension of **2** (50 mg, 0.08 mmol) in MeOH and the red mixture was stirred at room temp. for 18 h. The red product solution was evacuated to dryness and the residue extracted with toluene (2 × 3 mL). The extract was concentrated to about 2 mL and loaded on a silica gel column (1.5 × 2.0 cm). Elution gave three fractions: (i) a yellow eluate in ether/hexane (1:2, about 4 mL), which yielded [Ru(dppm)(η^1-S_2PR_2)$_2$] (R = Et (**15**), 3 mg, 5% yield, R = Ph (**17**), 3 mg, 4% yield), (ii) a red eluate in ether:hexane (2:1, 4–8 mL), which yielded [(Ind)Ru(dppm)(η^1-S_2PR_2)] (R = Et (**14**), 16 mg, 56% yield, R = Ph (**16**), 33 mg, 50% yield), (iii) an orange-yellow eluate in THF (3 mL), which gave **2** in trace amounts.

Data for 14: ^1H NMR (C_6D_6): δ = 1.07 and 1.11 [each t, $^3J_{HH}$ = 7.4 Hz, 3 H, $S_2P(CH_2CH_3)_2$], 1.46–1.57 [m, 4 H, $S_2P(CH_2CH_3)_2$], 4.04–4.16 and 4.43–4.54 [each m, 1 H, $CH_2(PPh_2)_2$], 5.15 (t, $^3J_{HH}$ = 2.5 Hz, 1 H, H^2), 6.12 (d, $^3J_{HH}$ = 2.5 Hz, 2 H, $H^{1,3}$), 6.89–7.12, 7.23–7.29, 7.37–7.43 and 7.78–7.81 (each m, total 24 H, H^{5-8} and Ph) ppm. $^{31}P\{^1H\}$ NMR (C_6D_6): δ = 12.5 (d, $^3J_{PP}$ = 19 Hz, d), 84.9 (t, $^3J_{PP}$ = 19 Hz, S_2PEt_2) ppm. IR (KBr): $\tilde{\nu}$ = 3052 (w), 2967 (w), 2927 (w), 1433 (m), 1324 (w), 1093 (m), 1027 (w), 730 [s, (PS)], 697 [vs, (PS)], 596 (m, (PS)], 534 m, 510 m. FAB^+-MS: m/z (%) = 791 $[M - Ind + S_2PEt_2]^+$, 639 $[M - Ind]^+$, 601 $[M - S_2PEt_2]^+$. $C_{38}H_{39}P_3RuS_2$ (753.84): calcd. C 60.5, H 5.2, S 8.5, found C 60.6, H 5.3, S 8.3.

Data for 15: ^1H NMR (C_6D_6): δ = 0.45–0.57 [m, 6 H, $S_2P(CH_2CH_3)_2$], 0.87–1.02 [m, 4 H, $S_2P(CH_2CH_3)_2$], 1.14–1.25 [m, 6 H, $S_2P(CH_2CH_3)_2$], 2.18–2.45 [m, 4 H, $S_2P(CH_2CH_3)_2$], 4.78–4.85 [m, 2 H, $CH_2(PPh_2)_2$], 6.91–7.34 and 8.10–8.16 (each m, total 20 H, Ph) ppm. $^{31}P\{^1H\}$ NMR (C_6D_6): δ = 5.1 (s, d), 105.6 (s, S_2PEt_2) ppm. IR (KBr): $\tilde{\nu}$ = 3049 (w), 2967 (w), 2929 (w), 2874 (w), 1433 (m), 1096 (m), 1036 (w), 723 [s, (PS)], 699 [vs, (PS)], 674, 603 [w, (PS)], 541 (m), 510 (m) cm^{-1}. FAB^+-MS: m/z (%) = 791 $[M]^+$, 639 $[M - S_2PEt_2]^+$. $C_{33}H_{42}P_4RuS_4$ (791.92): calcd. C 50.0, H 5.4, S 16.2, found C 50.2, H 5.4, S 15.7.

Data for 16: ^1H NMR (C_6D_6): δ = 3.94–4.06 and 4.42–4.54 [each m, 1 H, $CH_2(PPh_2)_2$], 5.15 (t, $^3J_{HH}$ = 2.5 Hz, 1 H, H^2), 5.82 (d, $^3J_{HH}$ = 2.5 Hz, 2 H, $H^{1,3}$), 6.66–6.69 (4-line m, 2 H, H^{4-7}), 6.90–7.11, 7.26–7.32, 7.47–7.53 and 8.13–8.20 [each m, total 32 H, S_2PPh_2, $CH_2(PPh_2)_2$, 2H of H^{5-8}] ppm. $^{31}P\{^1H\}$ NMR (C_6D_6): δ = 12.6 (d, $^3J_{PP}$ = 15 Hz, d), 70.9 (t, $^3J_{PP}$ = 19 Hz, S_2PPh_2) ppm. IR (KBr): $\tilde{\nu}$ = 3050 (w), 1481 (w), 1434 (s), 1306 (w), 1098 (s), 726 [m, (PS)], 703 [vs, (PS)], 568 [s, (PS)], 539 (m), 509 (m) cm^{-1}. FAB^+-MS: m/z (%) 850 $[M]^+$, 735 $[M - Ind]^+$, 601 $[M - S_2PPh_2]^+$. $C_{46}H_{39}P_3RuS_2$ (849.93): calcd. C 65.0, H 4.6, S 7.6, found C 65.2, H 5.0, S 7.7.

Data for 17: ^1H NMR (C_6D_6): δ = 4.76–4.82 [m, 2 H, $CH_2(PPh_2)_2$], 6.91–7.34, 8.08–8.26 (each m, total 40 H, Ph) ppm. $^{31}P\{^1H\}$ NMR (C_6D_6): δ = 4.0 (s, d), 88.0 (s, S_2PPh_2) ppm. IR (KBr): $\tilde{\nu}$ = 3049 (w), 2923 (w), 2854 (w), 1480 (w), 1433 (m), 1305 (w), 1097 (s), 1025 (w), 997 (w), 845 (w), 725 [s, (PS)], 703 [vs, (PS)], 631 (w), 608 (w), 567 [s, (PS)], 538 (m), 508 (m) cm^{-1}. FAB^+-MS: m/z (%) 984 $[M]^+$, 735 $[M - S_2PPh_2]^+$. $C_{49}H_{42}P_4RuS_4$ (984.09): calcd. C 59.8, H 4.3, S 13.0, found C 60.1, H 4.6, S 12.6.

(II) Reactions of (Ind)Ru(carbonyl) Complexes

(a) Reaction with Isopropyl Xanthate: A solution of [(Ind)Ru(CO)$_2$I] (**18**) (50 mg, 0.13 mmol) and $KS_2CO{i}Pr$ (45 mg, 0.26 mmol) in CH_3OH (15 mL) was stirred for 30 min at ambient temperature. The red solution slowly turned orange-yellow. Solvent was removed under vacuo and extracted with toluene (about 20 mL) to afford orange-red solids of [Ru(CO)$_2$(η^2-$S_2CO{i}Pr$)$_2$] (**19**) (24 mg, 50% yield).

Data for 19: ^1H NMR (C_6D_6): δ = 0.85 (m, 6 H, CH_3), 5.15 (sept, $^3J_{HH}$ = 6.1 Hz, 1 H, CH) ppm. ^{13}C NMR (C_6D_6): δ = 21.8 (CH_3),

78.0 (O-*C*H), 195.3 (S*C*O), 230.0 (*C*O) ppm. IR (THF): $\tilde{\nu}_{CO}$ = 2047 s, 1986 (s) cm^{-1} (literature[23] values 2052 s, 1990 s in C_6H_{12}). FAB^+-MS: 429.3 $[M + H]^+$.

(b) Reaction with Trimethylamine *N*-Oxide (TMNO): A solution of **18** (20.0 mg, 0.05 mmol) and TMNO·$2H_2O$ (12.0 mg, 0.11 mmol) in CH_3CN (10 mL) was stirred for 1 h at ambient temperature. The resulting dark brown solution was adsorbed onto Celite (150 mg). Solvent was removed under vacuo and the Celite mixture was loaded onto a silica gel column (5 × cm) prepared in *n*-hexane. Elution with toluene gave an orange-red solution (about 40 mL), which, upon removal of solvent to dryness, afforded a red solid of $[(Ind)Ru(CO)I]_2$ (**20**) (13 mg, 70% yield).

In a repeated reaction of the same scale, the resulting brown solution was evacuated to dryness. The residue was dissolved in C_6D_6 and filtered. The reddish brown filtrate was allowed to evaporate at room temperature. Analytical pure red microcrystals of **20** were obtained after 2 d (10 mg, 54% yield).

Data for 20: ^1H NMR (C_6D_6): δ = 4.26 (d, $^3J_{HH}$ = 2.5 Hz, 4 H, $H^{1,3}$), 4.37 (t, $^3J_{HH}$ = 2.5 Hz, 2 H, H^2), 6.54 (d, $^3J_{HH}$ = 8.2 Hz, 2 H, H^{5-8}), 6.77 (t, $^3J_{HH}$ = 8.1 Hz, 2 H, H^{5-8}), 6.90 (t, $^3J_{HH}$ = 7.9 Hz, 2 H, H^{5-8}), 7.59 (d, $^3J_{HH}$ = 8.2 Hz, 2 H, H^{5-8}) ppm. IR (KBr): $\tilde{\nu}_{CO}$ = 1925 (s) cm^{-1}. ESI^+-MS: 742.5 $[M]^+$. $C_{20}H_{14}I_2O_2Ru_2 \cdot 0.35C_6D_6$ (771.67): calcd. C 34.4, H 1.8, found C 34.8, H 2.3.

(c) Reaction with Diethyl Dithiocarbamate in the Presence of TMNO: A solution of **18** (30.0 mg, 0.08 mmol) and TMNO·$2H_2O$ (17.0 mg, 0.15 mmol) in CH_3CN (15 mL) was stirred for 30 min at ambient temperature. The resulting dark brown solution was transferred via a cannula into a flask containing $NaS_2CNEt_2 \cdot 3H_2O$ (17.0 mg, 0.80 mmol) and the mixture was stirred for 1 h, giving a dirty green solution. This was concentrated to about 10 mL and adsorbed onto Celite (200 mg). Solvent was removed under vacuo and the Celite mixture was loaded onto a silica gel column (5 × 2 cm) prepared in *n*-hexane. Elution gave a yellow eluate in toluene (about 25 mL), which, upon removal of solvent, afforded a yellow solid of $(Ind)Ru(CO)(\eta^2\text{-}S_2CNEt_2)$ (**21**) (16 mg, 55% yield).

Data for 21: ^1H NMR (C_6D_6): δ = 0.61 (t, $^3J_{HH}$ = 7.1 Hz, 6 H, N-CH_2CH_3), 2.94 (q, $^3J_{HH}$ = 7.1 Hz, 4 H, N-CH_2), 4.85 (t, $^3J_{HH}$ = 2.6 Hz, 1 H, H^2), 5.16 (d, $^3J_{HH}$ = 2.6 Hz, 2 H, $H^{1,3}$), 6.91–6.96 (4-line m, 2 H, H^{5-8}), 7.12–7.16 (m, 2 H, H^{5-8}) ppm. ^{13}C NMR (C_6D_6): δ = 11.7 (CH_3), 43.1 (N–CH_2), 64.6 ($C^{1,3}$), 85.8 (C^2), 113.1 ($C^{4,9}$), 124.4, 126.3 ($C^{5,8}$ and $C^{6,7}$), 201.5 (S*C*N), 215.3 (*C*O) ppm. IR (THF): $\tilde{\nu}_{CO}$ = 1931 (s) cm^{-1}. FAB^+-MS: 393.0 $[M]^+$, 364.9 [M – CO]$^+$. $C_{15}H_{17}NORuS_2$ (392.5): calcd. C 45.9, H 4.4, N 3.6, S 16.3, found C 45.8, H 4.2, N 3.2, S 16.0.

(d) Reaction with Isopropyl Xanthate in the Presence of TMNO: A similar reaction using KS_2CO*i*Pr (14.0 mg, 0.08 mmol) to replace $NaS_2CNEt_2 \cdot 3H_2O$ resulted in a brownish yellow solution. A similar chromatographic workup gave a yellow solution in toluene (about 25 mL), which, upon removal of solvent, afforded an orange oil. Recrystallization of the orange oil in hexane gave yellow crystals of $(Ind)Ru(CO)(\eta^2\text{-}S_2CO$*i*$Pr)$ (**22**) (23.0 mg, 81% yield).

Data of 22: ^1H NMR (C_6D_6): δ = 0.80 (d, $^3J_{HH}$ = 6.2 Hz, 6 H,CH_3), 4.77 (t, $^3J_{HH}$ = 2.6 Hz, 1 H, H^2), 5.00 (sept, $^3J_{HH}$ = 6.2 Hz, 1 H, O-C*H*), 5.07 (d, $^3J_{HH}$ = 2.6 Hz, 2 H, $H^{1,3}$), 6.83–6.87 (4-line m, 2 H, H^{5-8}), 6.95–6.98 (4-line m, 2 H, H^{5-8}) ppm. ^{13}C NMR (CD_2Cl_2): δ = 21.4 (CH_3), 65.1 ($C^{1,3}$), 76.8 (O-*C*H), 85.8 (C^2), 111.6 ($C^{4,9}$), 124.8, 127.4 ($C^{5,8}$ and $C^{6,7}$), 199.4 (S*C*O), 231.9 (*C*O) ppm. IR (THF): $\tilde{\nu}_{CO}$ = 2041 (s) cm^{-1}. EI-MS: 380.1 $[M]^+$, 352.0 [M – CO]$^+$, 217.0 [M – CO–$S_2COC_3H_7$]$^+$. HR-FAB^+-MS for $C_{14}H_{14}O_2RuS_2$ $[M]^+$: *m*/*z* (%) = 379.9563 (found), 379.9473 (calcd.), for $C_{13}H_{14}ORuS_2$ [M – CO]$^+$: *m*/*z* (%) = 351.9599 (found), 351.9524 (calcd.). $C_{14}H_{14}O_2RuS_2$ (379.46): calcd. C 44.3, H 3.7, S 16.9, found C 44.7, H 3.7, S 16.8.

Crystal Structure Determinations: X-ray diffraction-quality crystals were obtained at –30 °C from solvent mixtures as follows: **7**, **9**, **11**, **16**, and **17** from CH_2Cl_2/hexane, **4a** from CH_2Cl_2/ether and **12** from THF/hexane, while those of **20** and **21** were obtained at room temperature from C_6D_6 and CH_3CN/C_6D_6, respectively. Crystals were mounted on quartz fibers. X-ray data were collected on a Bruker AXS APEX system, using Mo-K_α radiation, with the SMART suite of programs.[24] Data were processed and corrected for Lorentz and polarization effects with SAINT,[25] and for absorption effects with SADABS.[26] Structural solution and refinement were carried out with the SHELXTL suite of programs.[27] Crystal and structure refinement data are summarized in Table 3. The structures were solved by direct methods or Patterson maps to locate the heavy atoms, followed by difference maps for the light, non-hydrogen atoms. All non-hydrogen atoms were generally given anisotropic displacement parameters in the final model.

The crystal of **4a** contains one and a half Et_2O solvent molecules. The half solvent molecule was disordered over two sites related by an inversion center, appropriate restraints on the molecular geometry were applied.

The crystal of **11** contained two half CH_2Cl_2 solvent molecules, both at special position and both disordered, while the crystal of **17** contained three CH_2Cl_2 solvent molecules. Two CH_2Cl_2 solvent molecules were also found and refined for **7** and **9**. The latter also contained a half molecule of hexane, which was modeled as disordered over two sites of equal occupancies, a common thermal parameter each for the CH_2 and CH_3 carbon atoms were assigned, with appropriate restraints on the bond lengths. The molecule of **7** exhibited disorder of the NEt_2 fragment over two alternative sites, the occupancies were allowed to refine and summed to unity, giving an approximate 65:35 ratio. The thermal parameters for the corresponding atoms were restrained to be the same, as were the bond lengths.

For complex **12**, two half molecules of THF were found. These were modeled with a common thermal parameter each for the O and C atoms, and with appropriate restraints on the bond lengths. The molecule of **12** exhibited disorder, which was modeled with two alternative sites for the Ru atom and the PEt_2 fragment. The occupancies were initially refined in an all-isotropic model and then fixed at 0.9 and 0.1 for the two sites, respectively, in the final model. Appropriate restraints similar to those described for the solvent molecule above were also applied. The molecular structure of **20** exhibits crystallographic mirror symmetry, with the mirror plane passing through the two Ru atoms and bisecting the Ru_2S_2 plane.

CCDC-626123 to -626131 contain the supplementary crystallographic data for this paper. These data can be obtained free of charge from The Cambridge Crystallographic Data Centre via www.ccdc.cam.ac.uk/data_request/cif.

Computation: The initial geometries of the ruthenium complexes used for the calculations were based on some of the X-ray crystal structures obtained. The structures of the reactants, products, and transition state were fully optimized at the B3LYP density functional theory together with LANL2DZ basis sets. Harmonic frequencies were calculated at the optimized geometries to characterize stationary points as equilibrium structures, with all real frequencies, or transition states with one imaginary frequency, and to evaluate zero-point energy (ZPE) corrections. For all cases in which transition states have been found, these states were verified by following the path traced by the reaction coordinate, which was the

Table 3. Crystal and structure refinement data.

Compound	**4a**·1.5(Et_2O)	**9**·2(CH_2Cl_2)·0.5(C_6H_{14})	**12**·(C_4H_8O)
Formula	$C_{54}H_{60}FeNO_{1.50}P_2RuS_2$	$C_{51}H_{51}Cl_4FeOP_2RuS_2$	$C_{51}H_{53}FeOP_3RuS_2$
Formula mass	1030.01	1104.70	995.88
Space group (crystal system)	$P\bar{1}$	$P\bar{1}$	$P\bar{1}$
Crystal system	triclinic	triclinic	triclinic
Unit cell dimensions			
a [Å]	13.7226(9)	11.6305(7)	11.3272(14)
b [Å]	13.7314(9)	14.5322(8)	13.4646(17)
c [Å]	14.4562(9)	15.8226(9)	16.962(2)
α [°]	75.104(2)	104.580(1)	105.351(3)
β [°]	69.530(2)	109.823(1)	94.667(3)
γ [°]	84.632(2)	95.273(1)	99.352(3)
Cell volume [Å^3]	2466.2(3)	2388.2(2)	2440.4(5)
Z	2	2	2
D_{calcd} (g/cm^3)	1.387	1.536	1.355
Absorption coefficient [mm^{-1}]	0.790	1.036	0.826
F(000) electrons	1070	1130	1028
Crystal size [mm^3]	0.29 × 0.10 × 0.04	0.32 × 0.24 × 0.11	0.28 × 0.20 × 0.12
θ range for data collection [°]	2.11–26.37	2.17–29.69	2.09–26.37
Index ranges	$-16 \le h \le 17$	$-16 \le h \le 14$	$-14 \le h \le 14$
	$-16 \le k \le 17$	$-20 \le k \le 18$	$-16 \le k \le 16$
	$0 \le l \le 18$	$0 \le l \le 21$	$0 \le l \le 21$
Reflections collected	33018	33852	31598
Independent reflections	10064	12251	9971
Max. and min. transmission	0.9691–0.8033	0.8945–0.7327	0.9074–0.8017
Data/restraints/parameters	10064/15/577	12251/4/555	9971/26/571
Gof	1.167	1.099	1.173
Final R indices [$I > 2\sigma(I)$]	R_1 = 0.0728	R_1 = 0.0484	R_1 = 0.0861
	wR_2 = 0.1325	wR_2 = 0.1162	wR_2 = 0.2272
R indices (all data)	R_1 = 0.1051	R_1 = 0.0540	R_1 = 0.1024
	wR_2 = 0.1434	wR_2 = 0.1203	wR_2 = 0.2371
Largest diff. peak and hole [e/Å^3]	1.058 and –0.591	1.462 and –0.893	1.512 and –1.322

Compound	**16**	**20**	**21**
Formula	$C_{47}H_{41}Cl_2P_3RuS_2$	$C_{10}H_7IORu$	$C_{15}H_{17}NORuS_2$
Formula mass	934.80	371.13	392.49
Space group (crystal system)	$P2_1/C$	$Pnma$	$P2_1/c$
Crystal system	monoclinic	orthorhombic	monoclinic
Unit cell dimensions			
a [Å]	11.4645(6)	19.462(2)	11.6373(9)
b [Å]	44.244(2)	9.5125(12)	7.1854(5)
c [Å]	8.3165(5)	19.7207(15)	19.7207(15)
α [°]	90	90	90
β [°]	90.321(2)	90	103.900(2)
γ [°]	90	90	90
Cell volume [Å^3]	4218.3(4)	1999.2(4)	1600.7(2)
Z	4	8	4
D_{calcd} (g/cm^3)	1.472	2.466	1.629
Absorption coefficient [mm^{-1}]	0.745	4.611	1.234
F(000) electrons	1912	1376	792
Crystal size [mm^3]	0.20 × 0.16 × 0.10	0.18 × 0.11 × 0.05	0.34 × 0.20 × 0.14
θ range for data collection [°]	0.92–25.00	2.09 to 26.37	1.80 to 27.49
Index ranges	$-11 \le h \le 13$	$0 \le h \le 24$	$-11 \le h \le 15$
	$-52 \le k \le 52$	$0 \le k \le 11$	$-9 \le k \le 9$
	$-9 \le l \le 9$	$0 \le l \le 13$	$-21 \le l \le 25$
Reflections collected	24515	12455	10941
Independent reflections	7415	2162	3648
Max. and min. transmission	0.9292–0.8653	0.8022–0.4908	0.8462–0.6790
Data/restraints/parameters	7415/0/496	2162/0/130	3648/0/183
Gof	1.310	1.335	1.172
Final R indices [$I > 2\sigma(I)$]	R_1 = 0.0916	R_1 = 0.0580,	R_1 = 0.0414
	wR_2 = 0.1609	wR_2 = 0.1698	wR_2 = 0.0985
R indices (all data)	R_1 = 0.1113	R_1 = 0.0580,	R_1 = 0.0460
	wR_2 = 0.1674	wR_2 = 0.1698	wR_2 = 0.1011
Largest diff. peak and hole [e/Å^3]	1.108 and –1.358	3.170 and –1.211	0.585 and –0.351

mode with the imaginary frequency. These displacements were indeed along the reaction pathways leading to the products (the η^3 complex) or back to the reactants (the η^5 complex). All calculations were performed using the Gaussian 03 suite of programs.[28]

Supporting Information (see also the footnote on the first page of this article): Table S1. Energies of selected molecules and transition states involved in the indenyl $\eta^5 \rightarrow \eta^3$ ring slippage process computed at B3LYP/LANL2DZ level of theory. Bond parameters of selected molecules and transition states involved in the indenyl $\eta^5 \rightarrow \eta^3$ ring slippage process computed at B3LYP/LANL2DZ level of theory. Table S2. Crystal and structure refinement data of complexes **7**, **11**, and **17**. Table S3. Selected bond lengths [Å] and angles [°] for complexes **7**, **11**, and **17**. ORTEP diagrams of **7**, **11**, and **17** with selected bond parameters.

Acknowledgments

The authors acknowledge with thanks support from the Academic Research Fund (grant no. 143-000-209-112 to L. Y. G, the Institute of Chemical and Engineering Sciences for a research scholarship to S. Y. N, and technical assistance from Dr. L. L. Koh and Ms G. K. Tan for X-ray structure determinations of **11**, **16**, **17**, and **21**.

[1] See for instance the following and references cited therein: a) G. Hogarth, *Prog. Inorg. Chem.* **2005**, *53*, 71, b) E. R. T. Tiekink, G. Winter, *Rev. Inorg. Chem.* **1992**, *12*, 185, c) G. Winter, *Rev. Inorg. Chem.* **1980**, *2*, 254, d) D. Coucouvanis, *Prog. Inorg. Chem.* **1979**, *26*, 302, e) R. Eisenberg, *Prog. Inorg. Chem.* **1970**, *12*, 295, f) D. Coucouvanis, *Prog. Inorg. Chem.* **1970**, *11*, 234, g) I. Haiduc, L. Y. Goh, *Coord. Chem. Rev.* **2002**, *1–2*, 151.

[2] Z. Weng, L. Y. Goh, *Acc. Chem. Res.* **2004**, *37*, 187, and references therein.

[3] a) X. L. Lu, J. J. Vittal, E. R. T. Tiekink, G. K. Tan, S. L. Kuan, L. Y. Goh, T. S. A. Hor, *J. Organomet. Chem.* **2004**, *689*, 1978, b) X. L. Lu, J. J. Vittal, E. R. T. Tiekink, L. Y. Goh, T. S. A. Hor, *J. Organomet. Chem.* **2004**, *689*, 1444.

[4] a) V. Cadierno, J. Díez, M. P. Gamasa, J. Gimeno, E. Latra, *Coord. Chem. Rev.* **1999**, *193–195*, 147, b) M. J. Calhorda, L. F. Veiros, *Coord. Chem. Rev.* **1999**, *185–186*, 37, c) J. M. O'Connor, C. P. Casey, *Chem. Rev.* **1987**, *87*, 307, d) R. T. Baker, T. H. Tulip, *Organometallics* **1986**, *5*, 839, e) J. W. Faller, R. H. Crabtree, A. Habib, *Organometallics* **1985**, *4*, 929, f) M. E. Rerek, L. N. Ji, F. Basolo, *J. Chem. Soc. Chem. Commun.* **1983**, 1208.

[5] See for instance the following: a) W. K. Fung, X. Huang, M. L. Man, S. M. Ng, M. Y. Hung, Z. Lin, C. P. Lau, *J. Am. Chem. Soc.* **2003**, *125*, 11539, b) M. K. Y. Watanabe, T. Ando, M. Sawamoto, *J. Am. Chem. Soc.* **2002**, *124*, 9994, c) T. Ando, M. Kamigito, M. Sawamoto, *Macromolecules* **2000**, *33*, 5825, d) E. P. Kündig, C. M. Saudan, V. Alezra, F. Viton, G. Bernardinelli, *Angew. Chem. Int. Ed.* **2001**, *40*, 4481, e) H. Takahashi, T. Ando, M. Kamigito, M. Sawamoto, *Macromolecules* **1999**, *32*, 3820, f) B. M. Trost, R. C. Livingston, *J. Am. Chem. Soc.* **1995**, *117*, 9586, g) B. M. Trost, R. J. Kulawiec, *J. Am. Chem. Soc.* **1993**, *115*, 2027.

[6] T. Sato, M. Nishio, Y. Ishii, H. Yamazaki, M. Hidai, *J. Organomet. Chem.* **1998**, *569*, 98.

[7] S. Y. Ng, W. K. Leong, L. Y. Goh, R. D. Webster, *Eur. J. Inorg. Chem.* **2007**, 463 and references cited therein.

[8] X. L. Lu, S. Y. Ng, J. J. Vittal, G. K. Tan, L. Y. Goh, T. S. A. Hor, *J. Organomet. Chem.* **2003**, *688*, 100.

[9] a) M. I. Bruce, M. G. Humphrey, A. G. Swincer, R. C. Wallis, *Aust. J. Chem.* **1984**, *37*, 1747, b) T. Wilczewski, M. Bocheńska, J. F. Biernat, *J. Organomet. Chem.* **1981**, *215*, 87.

[10] M. P. Gamasa, J. Gimeno, C. González-Bernardo, B. M. Martín-Vaca, J. Borge, S. García-Granda, *Inorg. Chim. Acta* **2003**, *347*, 181.

[11] a) S. D. Orth, N. R. Terry, K. A. Abboud, B. Dodson, L. McElwee-White, *Inorg. Chem.* **1996**, *35*, 916, b) B. Chaudret, G. Commernges, R. Poilblanc, *J. Chem. Soc. Dalton Trans.* **1984**, 1635.

[12] A. Shaver, P.-Y. Plouffe, P. Bird, E. Livingstone, *Inorg. Chem.* **1990**, *29*, 1826.

[13] S. L. Kuan, J. Tan, W. K. Leong, L. Y. Goh, Unpublished results.

[14] A. K. Kakkar, N. J. Taylor, T. B. Marder, J. K. Shen, N. Hallinan, F. Basolo, *Inorg. Chim. Acta* **1992**, *198–200*, 219, reported for true η^5-coordination: Δ = 0.03 Å, HA = 2.5°, FA = 4.4°, for distorted η^5: Δ = 0.11–0.42 Å, HA = 7–14°, FA = 6–13°, and for true η^3-coordination: Δ = 0.8 Å, FA = 28°. In general, for indenyl complexes considered η^5: $\Delta < 0.25$ Å, HA < 10°, and for those considered η^3: Δ = 0.69–0.80 Å, HA ≈ 20–30°, and for those with slight distortion towards η^3: Δ = 0–0.22 Å, HA < 13° (see for instance, refs.[4a,4b] and M. E. Stoll, P. Belanzoni, M. J. Calhorda, M. G. B. Drew, V. Félix, W. E. Geiger, C. A. Gamelas, I. S. Goncalves, C. C. Romão, L. F. Veiros, *J. Am. Chem. Soc.* **2001**, *123*, 10595).

[15] L. Pauling, *The Nature of the Chemical Bond*, Cornell University Press, Ithaca, NY, **1960**, chapter 8.

[16] a) A. J. Deeming, C. Forth, G. Hogarth, *J. Organomet. Chem.* **2006**, *691*, 79, b) J. D. Owen, D. J. Cole-Hamilton, *J. Chem. Soc. Dalton Trans.* **1974**, 1867.

[17] M. S. Loonat, L. Carlton, J. C. A. Boeyens, M. J. Covelle, *J. Chem. Soc. Dalton Trans.* **1989**, 2407.

[18] H. W. Vos, C. MacLean, N. H. Velthorst, *J. Chem. Soc. Faraday Trans.* **1976**, *72*, 63.

[19] M. J. Calhorda, C. C. Romão, L. F. Veiros, *Chem. Eur. J.* **2002**, *8*, 868.

[20] S. Y. Ng, G. Fang, W. K. Leong, L. Y. Goh, M. Garland, *Eur. J. Inorg. Chem.* **2007**, 452.

[21] M. P. Gamasa, J. Gimeno, C. Gonzalez-Bernardo, B. M. Martin-Vaca, D. Monti, M. Bassetti, *Organometallics* **1996**, *15*, 302.

[22] P. McArdle, A. R. Manning, *J. Chem. Soc. A* **1970**, 2128.

[23] A. J. Deeming, C. Forth, G. Hogarth, *Transition Met. Chem.* **2006**, *31*, 42.

[24] *SMART* version 5.628, Bruker AXS Inc., Madison, WI, USA, **2001**.

[25] *SAINT+* version 6.22a, Bruker AXS Inc., Madison, WI, USA, **2001**.

[26] G. M. Sheldrick, *SADABS*, **1996**.

[27] *SHELXTL* version 5.1, Bruker AXS Inc., Madison, WI, USA, **1997**.

[28] M. J. Frisch, G. W. Trucks, H. B. Schlegel, G. E. Scuseria, M. A. Robb, J. R. Cheeseman, J. A. Montgomery, Jr., T. Vreven, K. N. Kudin, J. C. Burant, J. M. Millam, S. S. Iyengar, J. Tomasi, V. Barone, B. Mennucci, M. Cossi, G. Scalmani, N. Rega, G. A. Petersson, H. Nakatsuji, M. Hada, M. Ehara, K. Toyota, R. Fukuda, J. Hasegawa, M. Ishida, T. Nakajima, Y. Honda, O. Kitao, H. Nakai, M. Klene, X. Li, J. E. Knox, H. P. Hratchian, J. B. Cross, C. Adamo, J. Jaramillo, R. Gomperts, R. E. Stratmann, O. Yazyev, A. J. Austin, R. Cammi, C. Pomelli, J. W. Ochterski, P. Y. Ayala, K. Morokuma, G. A. Voth, P. Salvador, J. J. Dannenberg, V. G. Zakrzewski, S. Dapprich, A. D. Daniels, M. C. Strain, O. Farkas, D. K. Malick, A. D. Rabuck, K. Raghavachari, J. B. Foresman, J. V. Ortiz, Q. Cui, A. G. Baboul, S. Clifford, J. Cioslowski, B. B. Stefanov, G. Liu, A. Liashenko, P. Piskorz, I. Komaromi, R. L. Martin, D. J. Fox, T. Keith, M. A. Al-Laham, C. Y. Peng, A. Nanayakkara, M. Challacombe, P. M. W. Gill, B. Johnson, W. Chen, M. W. Wong, C. Gonzalez, J. A. Pople, *Gaussian 03*, Gaussian Inc., Wallingford CT, **2004**..

Received: January 20, 2007
Published Online: June 29, 2007

